A positivity preserving and oscillation-free entropy stable discontinuous Galerkin scheme for the reactive Euler equations

Zuo, Hujian; Zhao, Weifeng; Lin, Ping

Published in:
Journal of Computational Physics

DOI:
10.1016/j.jcp.2024.112906

Publication date:
2024

A positivity preserving and oscillation-free entropy stable discontinuous Galerkin scheme for the reactive Euler equations

Hujian Zuo

Department of Applied Mathematics, University of Science and Technology Beijing, Beijing 100083, China

Weifeng Zhao*

Department of Applied Mathematics, University of Science and Technology Beijing, Beijing 100083, China

Ping Lin*

Division of Mathematics, University of Dundee, Dundee, DD1 4HN, Scotland, United Kingdom

Abstract

The reactive Euler equations are a basic model for fluid flows with chemical reactions. In this work, we construct a high order positivity preserving and oscillation-free entropy stable discontinuous Galerkin (DG) scheme for the reactive Euler equations. The main ingredients of the scheme include (i) entropy preserving and entropy stable fluxes to achieve entropy stability, (ii) artificial damping terms to restrain spurious oscillations near the shocks, and (iii) positivity preserving limiters to guarantee the positivity of solutions. These ingredients are compatible with each other so that our scheme simultaneously enjoys the properties of entropy stable, oscillation-free and positivity preserving. Another distinctive feature of our scheme is that it is entropy stable for both the thermodynamic and mathematical entropies. Numerical experiments validate the designed high convergence orders of the scheme and demonstrate its good performances for discontinuous problems.

Keywords: Reactive Euler equations, discontinuous Galerkin method, entropy stable, oscillation-free, positivity preserving.

1. Introduction

The reactive Euler equations are an important model describing fluid flows with chemical reactions, *e.g.* , material combustion and gas detonations, and have attracted much attention in both mathematical theory and numerical simulations; see *e.g.* [1, 2, 3, 4, 5, 6, 7, 8]. Since

*Corresponding author

Email addresses: hjzuo@stu.pku.edu.cn (Hujian Zuo), wfzhao@ustb.edu.cn (Weifeng Zhao), plin@maths.dundee.ac.uk (Ping Lin)

the reactive Euler equations are a hyperbolic system, their solutions can be discontinuous in the presence of shocks or contact discontinuities. This leads to the consideration of weak solutions, which, however, may not be unique. To select the unique physical relevant solution among various weak solutions, entropy conditions are usually imposed as the admissibility criterion. As a result, it is natural to design numerical schemes preserving the entropy conditions of the reactive Euler equations.

On the other hand, it is frequently encountered in simulations that the density or pressure of the numerical solutions becomes negative. For example, for the gas detonation propagation through different geometries, the shock diffraction may result in very low density and pressure. In this case numerical schemes can easily produce negative density or pressure, even for non-reactive gas flows, and eventually lead to blow-ups [9]. It is thus necessary to simultaneously preserve the entropy conditions and the positivity of solutions in simulations [10].

Schemes satisfying entropy conditions are usually referred as entropy stable schemes. Such schemes for hyperbolic conservation laws have been well developed in the finite volume (finite difference) framework since the pioneer work of Osher and Tadmor [11, 12, 13]. Within this framework, a two-point entropy conservative (EC) numerical flux is derived first by choosing a suitable set of algebraic variables and then a dissipation term is added to obtain an entropy stable (ES) flux [12]. Using these fluxes as building blocks, one can design high-order EC/ES schemes following the procedure in [14]. Nevertheless, how to guarantee the positivity of solutions in this framework is still a challenge. More specifically, it is not clear whether the entropy stable fluxes thus obtained are positivity preserving in the sense of [15]. If these entropy stable fluxes are also positivity preserving, then the positivity preserving limiters in [15] can be employed.

Another popular category of entropy stable schemes is based on the discontinuous Galerkin

(DG) method [16]. Classical DG schemes only satisfy the square entropy inequality for scalar conservation laws and symmetric hyperbolic systems [17, 18]. In [19], Chen and Shu constructed a new framework for quadrature-based DG methods on conforming simplex meshes. By introducing special Gauss-Lobatto type quadrature rules with collocated surface quadrature points, they establish discrete matrices with summation-by-parts (SBP) property [20, 21]. Using these SBP matrices, along with entropy conservative fluxes and entropy stable fluxes [12], the designed DG schemes admit the entropy condition for a given entropy function. Additionally, the schemes are compatible with positivity preserving limiters developed in [22, 23, 24, 9]. Namely, imposing such limiters does not destroy the entropy stability. However, the stabilization of these schemes due to entropy dissipation produced by entropy stable fluxes is not enough and thus evident spurious oscillations may still generate in discontinuous problems [19]. To address this issue, Liu *et al.* improved this framework by adding entropy stable damping terms to the original one [25]. Such damping terms are originally proposed in [26, 27] for scalar conservation laws and hyperbolic systems without considering entropy stability, and recently they have been adapted to different equations thanks to their ability to control spurious oscillations and the convenience for theoretical analysis [28, 29, 30]. The entropy stable DG schemes implemented with the damping terms in [25], named oscillation-free entropy stable DG (ESOFDG) schemes, can restrain most oscillations in simulations while maintaining conservation, high order accuracy and entropy stability. Further development of the entropy stable DG schemes based on SBP operators in [19] can be found in [31, 32, 33, 34, 35, 36, 37, 38, 34, 39, 40, 41].

In this work, we consider entropy stable and positivity preserving schemes for the reactive Euler equations with the equation of state (EoS) for the ideal gas. Under this EoS, it is shown in [42] that the classical entropy function associated with the thermodynamic entropy is no

longer strictly convex. To remedy this, a new strictly convex entropy function is proposed by adding an extra term to the classical one [42]. The entropy stability with respect to the thermodynamic entropy indicates the second law of thermodynamics while that with respect to the strictly convex entropy is crucial for the wellposedness of solutions [43]. In this sense, the two entropy functions, termed thermodynamic entropy and mathematical entropy for short, are important from the physical and mathematical aspects, respectively. Thus here we aim to construct schemes that are entropy stable for both entropy functions, while keeping the positivity of solutions.

To achieve the above goal, we follow the framework of DG methods in [19, 25], the main task of which is to specify the entropy conservative and entropy stable fluxes. Here we choose the flux proposed in [42] as the entropy conservative flux and the HLL (Harten-Lax-van Leer) flux [44] as the entropy stable flux. We prove that the flux in [42] is entropy conservative for both the thermodynamic and mathematical entropies and the HLL flux is entropy stable for both entropies under suitable estimations for the wave speeds. In this way, the DG scheme we obtain is entropy stable for both the thermodynamic and mathematical entropies. Additionally, damping terms are added as in [25] to restrain oscillations and the positivity preserving limiters in [9] are imposed to guarantee the positivity of the density, pressure and mass fraction. These ingredients are compatible with each other so that our scheme simultaneously enjoys the properties of entropy stable, oscillation-free and positivity preserving. We test the scheme via various 1D and 2D examples. The numerical results not only validate the designed high convergence orders of the scheme and but also demonstrate its good performances for discontinuous problems. Some extreme problems are also employed to show the necessity of positivity preserving limiters.

We would like to point out that, as far as we aware, this is the first time that a numerical

scheme is entropy stable for both the thermodynamic and mathematical entropies. Namely, the scheme admits the discrete versions of the entropy conditions for both entropy functions. Since the entropy condition for the thermodynamic entropy corresponds to the second law of thermodynamics and that for the mathematical entropy is crucial for the wellposedness of solutions, such scheme is meaningful in both physics and mathematics. From this point of view, our scheme should be reliable in predicting complex detonation problems. We hope to extend the scheme to 3D and apply it to real applications in the future.

The rest of the paper is organized as follows. In Section 2, we briefly introduce the reactive Euler equations and some related entropy theory knowledge. In Section 3, we extend the framework in [19] to 1D reactive Euler equations. Related theories are given in this section. Furthermore, the entropy stable damping term [25] is used in this section to control the spurious oscillations. In Section 4, we adapt the positivity preserving limiter to our scheme. Section 5 introduces the time stepping methods implemented in this paper and the method in extending our scheme into two dimensional (2D) cases. Section 6 provides some numerical experiments to validate our schemes. Finally, some conclusions and remarks are given in Section 7. This paper also contains an appendix which gives the proofs of some theorems.

2. Reactive Euler equations and entropy functions

In one dimension, the reactive Euler equations read as

$$\mathbf{u}_t + \mathbf{f}(\mathbf{u})_x = \mathbf{s}(\mathbf{u}) \tag{2.1}$$

with

$$\mathbf{u} = \begin{pmatrix} \rho \\ \rho u \\ \rho E \\ \rho Y \end{pmatrix}, \mathbf{f}(\mathbf{u}) = \begin{pmatrix} \rho u \\ \rho u^2 + p \\ (\rho E + p)u \\ \rho u Y \end{pmatrix}, \mathbf{s}(\mathbf{u}) = \begin{pmatrix} 0 \\ 0 \\ 0 \\ Q \end{pmatrix}. \tag{2.2}$$

Here ρ, u, E, p, Y denote the fluid density, velocity, total energy per unit mass, pressure and reactant mass fraction, respectively. The source term $Q \leq 0$ characterizes the chemical reaction and is assumed to be the Arrhenius form

$$Q = -\widetilde{K}\rho Y e^{-\widetilde{T}/T}, \tag{2.3}$$

where $T = \frac{p}{\rho}$ is the temperature, $\tilde{T} > 0$ is the constant activation temperature and $\tilde{K} > 0$ is a constant rate coefficient. Throughout the paper, we adopt the equation of state for the ideal gas

$$\rho E = \frac{1}{2}\rho u^2 + \frac{p}{\gamma - 1} + q\rho Y,$$

where γ is the specific heat ratio and q is the heat release of reaction. We note that Q and q are not directly related.

Under the above equation of state, the classical entropy-entropy flux pair $(\hat{U}, \hat{\phi})$ is

$$\hat{U} = \frac{-\rho s}{\gamma - 1}, \quad \hat{\phi} = \frac{-\rho u s}{\gamma - 1}, \tag{2.4}$$

where $s = \ln(p\rho^{-\gamma})$ is the thermodynamic entropy. The entropy $\hat{U}$ is strictly convex for the Euler equations without chemical reactions. However, as pointed out in [42], $\hat{U}$ is not strictly convex at any states for the reactive Euler equations (2.1). To address this issue, a new entropy-entropy flux pair (U, ϕ) is proposed in [42], where

$$U = \hat{U} + \rho Y^2, \quad \phi = \hat{\phi} + \rho u Y^2. \tag{2.5}$$

It is shown in [42] that the new entropy function U is strictly convex and satisfies

$$\partial_t U + \partial_x \phi = (q\frac{\rho}{p} + 2Y)Q \leq 0.$$

The corresponding entropy variable is

$$\mathbf{v} := U'(\mathbf{u}) = \begin{pmatrix} \frac{\gamma-s}{\gamma-1} - \frac{\rho u^2}{2p} - Y^2 \\ \frac{\rho u}{p} \\ -\frac{\rho}{p} \\ q\frac{\rho}{p} + 2Y \end{pmatrix}, \tag{2.6}$$

and the entropy potential is

$$\psi := \mathbf{v}^T\mathbf{f} - \phi = \rho u. \tag{2.7}$$

3. Oscillation-free entropy stable DG scheme

In this section, we follow [25] and [19] to construct an oscillation-free entropy stable DG scheme for the reactive Euler equations (2.1). For simplicity we introduce the scheme detailedly for 1D problems and it can be extended to two dimensions directly.

To begin with, we assume the computational domain Ω is periodic or compactly supported, and has a regular partition

$$\Omega = \bigcup_{i=1}^{N} I_i, \tag{3.1}$$

where

$$I_i = \left[x_{i-\frac{1}{2}}, x_{i+\frac{1}{2}}\right], \quad x_{\frac{1}{2}} < x_{\frac{3}{2}} < \cdots < x_{N+\frac{1}{2}}, \quad \Delta x_i = x_{i+\frac{1}{2}} - x_{i-\frac{1}{2}}. \tag{3.2}$$

In addition, throughout this section we assume numerical solutions are within the admissible state set

$$G = \left\{\mathbf{u} \in \mathbf{R}^4 \mid \rho > 0, p(\mathbf{u}) > 0, Y \geqslant 0\right\}. \tag{3.3}$$

This assumption on the positivity is introduced to theoretically prove the entropy stability of the scheme and it will be guaranteed by positivity preserving limiters in the next section.

3.1. SBP matrices and nodal DG scheme

Set the discrete DG space as

$$\mathbf{V}_h^k = \left\{\mathbf{v}_h(x) : \mathbf{v}_h(x)|_{I_i} \in [\mathcal{P}^k(I_i)]^4, 1 \leq i \leq N\right\}, \tag{3.4}$$

where $\mathcal{P}^k(I_i)$ denotes the polynomials of degree not greater than k over the subintervals I_i. According to the DG theories, we aim to find the function $\mathbf{u}_h(\cdot,t) \in \mathbf{V}_h^k$ such that

$$\begin{aligned}\int_{I_i} (\mathbf{u}_h)_t \mathbf{v}_h dx - \int_{I_i} \mathbf{f}(\mathbf{u}_h) \frac{d\mathbf{v}_h}{dx} dx = \\ -\widehat{\mathbf{f}}_{i+\frac{1}{2}} \mathbf{v}_h\left(x_{i+\frac{1}{2}}^-\right) + \widehat{\mathbf{f}}_{i-\frac{1}{2}} \mathbf{v}_h\left(x_{i-\frac{1}{2}}^+\right) + \int_{I_i} \mathbf{s}(\mathbf{u}_h)\mathbf{v}_h dx, \forall \mathbf{v}_h \in \mathbf{V}_h^k\end{aligned} \tag{3.5}$$

on each subinterval I_i, where $\widehat{\mathbf{f}}_{i+\frac{1}{2}} = \widehat{\mathbf{f}}(\mathbf{u}_h(x_{i+\frac{1}{2}}^-), \mathbf{u}_h(x_{i+\frac{1}{2}}^+))$ is some numerical flux constructed with $\mathbf{u}_h(x_{i+\frac{1}{2}}^-)$ and $\mathbf{u}_h(x_{i+\frac{1}{2}}^+)$, the solutions at the left and right side of $x_{i+\frac{1}{2}}$, respectively.

To compute the integral in (3.5), we employ the Gauss-Lobatto quadrature. Specifically, let $-1 = \xi_0 < \xi_1 < \cdots < \xi_k = 1$ be the $k+1$ Gauss-Lobatto quadrature points on the reference element $I = [-1,1]$ and $\{\omega_j\}_{j=0}^k$ the corresponding quadrature weights. Define the Lagrange nodal basis

$$L_j(\xi) = \prod_{\substack{l=0 \\ l\neq j}}^{k} \frac{\xi - \xi_l}{\xi_j - \xi_l} \tag{3.6}$$

and denote the continuous and discrete product as

$$\langle u, v\rangle = \int_{-1}^{1} uv d\xi, \quad \langle u, v\rangle_\omega = \sum_{j=0}^{k} \omega_j u(\xi_j) v(\xi_j). \tag{3.7}$$

With these, we define the difference matrix D, the boundary matrix B, the mass matrix M and the stiffness matrix S as in [19]:

$$\begin{aligned} &D_{jl} := L_l'(\xi_j), \\ &B := \mathrm{diag}\{\tau_0, \tau_1, \cdots, \tau_k\} = \mathrm{diag}\{-1, 0, \cdots, 0, 1\}, \\ &M := \mathrm{diag}\{\omega_0, \omega_1, \cdots, \omega_k\}, \\ &S_{jl} := \langle L_j, L_l'\rangle_\omega = \langle L_j, L_l'\rangle. \end{aligned} \tag{3.8}$$

Here the last equation is because that the product $\langle u, v\rangle_\omega$ is exact for the polynoimals of degree not greater than $2k-1$. According to [19], the matrices defined in (3.8) have the

SBP properties, which are discrete analogues of integration by parts. These properties are essential in proving the entropy stability of the designed schemes.

Furthermore, for each interval I_i, we transform it into the element $[-1,1]$:

$$x_i(\xi) := \frac{\Delta x_i}{2}\xi + \frac{1}{2}\left(x_{i-\frac{1}{2}} + x_{i+\frac{1}{2}}\right), \quad 1 \le i \le N. \tag{3.9}$$

Then we denote

$$\begin{aligned}
\overrightarrow{\mathbf{u}^{i,m}} &:= \left[\ \mathbf{u}_h^m\left(x_i\left(\xi_0\right),t\right) \quad \cdots \quad \mathbf{u}_h^m\left(x_i\left(\xi_k\right),t\right)\ \right]^T, \\
\overrightarrow{\mathbf{f}^{i,m}} &:= \left[\ \mathbf{f}^m\left(\mathbf{u}_h\left(x_i\left(\xi_0\right),t\right)\right) \quad \cdots \quad \mathbf{f}^m\left(\mathbf{u}_h\left(x_i\left(\xi_k\right),t\right)\right)\ \right]^T, \\
\overrightarrow{\mathbf{f}_*^{i,m}} &:= \left[\ \widehat{\mathbf{f}}_{i-\frac{1}{2}}^m \quad 0 \quad \cdots \quad 0 \quad \widehat{\mathbf{f}}_{i+\frac{1}{2}}^m\ \right]^T, \\
\overrightarrow{\mathbf{s}^{i,m}} &:= \left[\ \mathbf{s}^m\left(\mathbf{u}_h\left(x_i\left(\xi_0\right),t\right)\right) \quad \cdots \quad \mathbf{s}^m\left(\mathbf{u}_h\left(x_i\left(\xi_k\right),t\right)\right)\ \right]^T,
\end{aligned} \tag{3.10}$$

where $1 \le m \le 4$, $1 \le i \le N$, and $\mathbf{Q}^m$ is the m-th component of $\mathbf{Q}$ with $\mathbf{Q} = \mathbf{u}_h$, $\mathbf{f}(\mathbf{u})$, $\widehat{\mathbf{f}}_{i\pm\frac{1}{2}}$ and $\mathbf{s}(\mathbf{u})$. With notations (3.6), (3.8) and (3.10), the formulation (3.5) can be converted into

$$\frac{\Delta x_i}{2}\frac{d\overrightarrow{\mathbf{u}^{i,m}}}{dt} + D\overrightarrow{\mathbf{f}^{i,m}} = M^{-1}B(\overrightarrow{\mathbf{f}^{i,m}} - \overrightarrow{\mathbf{f}_*^{i,m}}) + \frac{\Delta x_i}{2}\overrightarrow{\mathbf{s}^{i,m}}, \quad 1 \le m \le 4, \quad 1 \le i \le N. \tag{3.11}$$

Taking Kronecker product for the matrices in (3.8) as

$$\mathbf{M} = M \otimes I,\ \mathbf{D} = D \otimes I,\ \mathbf{B} = B \otimes I \tag{3.12}$$

with $I = \mathrm{diag}\{1,1,1,1\}$ and defining

$$\begin{aligned}
\overrightarrow{\mathbf{u}^i} &= \left[\ \mathbf{u}_h\left(x_i\left(\xi_0\right),t\right) \quad \cdots \quad \mathbf{u}_h\left(x_i\left(\xi_k\right),t\right)\ \right]^T, \\
\overrightarrow{\mathbf{f}^i} &= \left[\ \mathbf{f}\left(\mathbf{u}_h\left(x\left(\xi_0\right),t\right)\right) \quad \cdots \quad \mathbf{f}\left(\mathbf{u}_h\left(x_i\left(\xi_k\right),t\right)\right)\ \right]^T, \\
\overrightarrow{\mathbf{f}_*^i} &= \left[\ \widehat{\mathbf{f}}_{i-1/2} \quad 0 \quad \cdots \quad 0 \quad \widehat{\mathbf{f}}_{i+1/2}\ \right]^T, \\
\overrightarrow{\mathbf{s}^i} &= \left[\ \mathbf{s}\left(\mathbf{u}_h\left(x_i\left(\xi_0\right),t\right)\right) \quad \cdots \quad \mathbf{s}\left(\mathbf{u}_h\left(x_i\left(\xi_k\right),t\right)\right)\ \right]^T
\end{aligned} \tag{3.13}$$

for $1 \le i \le N$, we further write (3.11) as

$$\frac{\Delta x_i}{2}\frac{d\overrightarrow{\mathbf{u}^i}}{dt} + \mathbf{D}\,\overrightarrow{\mathbf{f}^i} = \mathbf{M}^{-1}\mathbf{B}(\overrightarrow{\mathbf{f}^i} - \overrightarrow{\mathbf{f}_*^i}) + \frac{\Delta x_i}{2}\overrightarrow{\mathbf{s}^i}. \tag{3.14}$$

This is the standard nodal DG scheme for the reactive Euler equations.

3.2. Entropy stable nodal DG scheme

Based on the standard nodal DG scheme (3.14), we follow [19] to construct entropy stable schemes. Before this, we introduce the definitions of entropy preserving flux and entropy stable flux [12, 13].

Definition 3.1 (Entropy preserving flux)**.** *A consistent, two-point symmetric numerical flux* $\widetilde{\mathbf{f}}(\mathbf{u}_L, \mathbf{u}_R)$ *for a given entropy function* η *is entropy preserving if*

$$(\mathbf{v}_R - \mathbf{v}_L)^T \widetilde{\mathbf{f}}\,(\mathbf{u}_L, \mathbf{u}_R) = \psi_R - \psi_L, \tag{3.15}$$

where $\mathbf{v}_{L,R}$ *and* $\psi_{L,R}$ *are the corresponding entropy variables and potential fluxes at the left and right states.*

Definition 3.2 (Entropy stable flux)**.** *A consistent, two-point numerical flux* $\widehat{\mathbf{f}}\,(\mathbf{u}_L, \mathbf{u}_R)$ *is entropy stable for a given entropy function* η *if*

$$(\mathbf{v}_R - \mathbf{v}_L)^T \widehat{\mathbf{f}}\,(\mathbf{u}_L, \mathbf{u}_R) \leq \psi_R - \psi_L. \tag{3.16}$$

With the above definitions, we denote

$$\begin{aligned} &\mathbf{u}_j^i = \mathbf{u}_h(x_i(\xi_j), t),\ \mathbf{f}_j^i = \mathbf{f}(\mathbf{u}_h(x_i(\xi_j), t)),\ \mathbf{s}_j^i = \mathbf{s}(\mathbf{u}_h(x_i(\xi_j), t)), \\ &\mathbf{f}_{*,j}^i = \begin{cases} \hat{\mathbf{f}}_{i-1/2}, & j = 0, \\ \hat{\mathbf{f}}_{i+1/2}, & j = k, \\ 0, & 1 \leq j \leq k-1, \end{cases} \end{aligned} \tag{3.17}$$

and modify the standard nodal DG scheme scheme (3.14) as

$$\frac{\Delta x_i}{2}\frac{d\mathbf{u}_j^i}{dt} + 2\sum_{l=0}^{k} D_{jl}\widetilde{\mathbf{f}}\left(\mathbf{u}_j^i, \mathbf{u}_l^i\right) = \frac{\tau_j}{\omega_j}(\mathbf{f}_j^i - \mathbf{f}_{*,j}^i) + \frac{\Delta x_i}{2}\mathbf{s}_j^i. \tag{3.18}$$

Here $\widetilde{\mathbf{f}}(\cdot,\cdot)$ is an entropy preserving flux and $\hat{\mathbf{f}}(\cdot,\cdot)$ in $\mathbf{f}^i_{*,j}$ is an entropy stable flux. In this way, the scheme (3.18) is entropy stable for entropy η in the sense that

$$\frac{d}{dt}\left(\sum_{i=1}^{N}\sum_{j=0}^{k}\frac{\Delta x_i}{2}\omega_j\eta^i_j\right)\leq\sum_{i=1}^{N}\sum_{j=0}^{k}\frac{\Delta x_i}{2}\omega_j\eta^{'}(\mathbf{u}^i_j)^4Q^i_j \tag{3.19}$$

for periodic or compactly supported boundary conditions, where $\eta^{'}(\mathbf{u}^i_j)^4$ stands for the 4-th component of the derivative of η with respect to $\mathbf{u}^i_j$.

Next we show how to choose the entropy preserving and entropy stable fluxes. Actually, for the reactive Euler equations (2.1), two sets of entropy preserving flux have been proposed in [42] for the mathematical entropy function U in (2.5). Here we adopt the one that preserves both the entropy equality and the kinetic energy equality. This flux is a generalization of the entropy conservative and kinetic energy preserving flux in [45] for the compressible Euler equations. Let a_L and a_R be the values of some variable a at the left and right states, respectively. Denote

$$[\![a]\!]=a_R-a_L,\quad \{\{a\}\}=\frac{1}{2}\left(a_L+a_R\right)$$

and introduce the logarithmic average

$$\{\{a\}\}^{\ln}=\frac{[\![a]\!]}{[\![\ln(a)]\!]}.$$

With algebraic variables

$$z=\begin{pmatrix}z^1\\z^2\\z^3\\z^4\end{pmatrix}=\begin{pmatrix}\rho\\u\\\underline{\rho}\\\underline{p}\\Y\end{pmatrix}, \tag{3.20}$$

the entropy preserving flux is [42]

$$\begin{aligned}
\tilde{\mathbf{f}}^1&=\left\{\left\{z^1\right\}\right\}^{\ln}\left\{\left\{z^2\right\}\right\},\\
\tilde{\mathbf{f}}^2&=\frac{\left\{\left\{z^1\right\}\right\}}{\left\{\left\{z^3\right\}\right\}}+\left\{\left\{z^2\right\}\right\}\tilde{\mathbf{f}}^1,\\
\tilde{\mathbf{f}}^3&=\left(\frac{1}{(\gamma-1)\left\{\left\{z^3\right\}\right\}^{\ln}}-\frac{1}{2}\left\{\left\{\left(z^2\right)^2\right\}\right\}\right)\tilde{\mathbf{f}}^1+\left\{\left\{z^2\right\}\right\}\tilde{\mathbf{f}}^2+q\tilde{\mathbf{f}}^4,\\
\tilde{\mathbf{f}}^4&=\left\{\left\{z^4\right\}\right\}\tilde{\mathbf{f}}^1,
\end{aligned} \tag{3.21}$$

where $\tilde{\mathbf{f}}^i$ is the i-th component of $\widetilde{\mathbf{f}}(\mathbf{u}_L, \mathbf{u}_R)$. On this flux, we have the following observation.

Lemma 3.1. *The numerical flux* (3.21) *is entropy preserving for both the the mathematical entropy U and the thermodynamic entropy $\hat{U}$.*

Proof. Since the proof for the mathematical entropy U has been given in [42], we only prove that (3.21) is entropy preserving for the thermodynamic entropy $\hat{U}$. For this entropy, the entropy variable is

$$\hat{\mathbf{v}} = \hat{U}'(\mathbf{u}) = \begin{pmatrix} \frac{\gamma - s}{\gamma - 1} - \frac{\rho u^2}{2p} \\ \frac{\rho u}{p} \\ -\frac{\rho}{p} \\ q\frac{\rho}{p} \end{pmatrix} \tag{3.22}$$

and entropy potential is $\hat{\psi} = \hat{\mathbf{v}}^T \mathbf{f} - \hat{\phi} = \rho u$.

We first recall from [46] that for the Euler equations without chemical reactions, the entropy variable $\mathbf{v}_{Euler}$ corresponding the thermodynamic entropy $\hat{U}$ is

$$\mathbf{v}_{Euler} = \begin{pmatrix} \frac{\gamma - s}{\gamma - 1} - \frac{\rho u^2}{2p} \\ \rho u / p \\ -\rho / p \end{pmatrix} \tag{3.23}$$

and the entropy conservative (preserving) flux is

$$\widetilde{\mathbf{f}}_{Euler}(\mathbf{u}_L, \mathbf{u}_R) = \begin{pmatrix} \{\{z^1\}\}^{\ln} \{\{z^2\}\} \\ \frac{\{\{z^1\}\}}{\{\{z^3\}\}} + \{\{z^2\}\} \widetilde{\mathbf{f}}^1 \\ \left(\frac{1}{(\gamma - 1)\{\{z^3\}\}^{\ln}} - \frac{1}{2} \left\{ \left\{ (z^2)^2 \right\} \right\} \right) \widetilde{\mathbf{f}}^1 + \{\{z^2\}\} \widetilde{\mathbf{f}}^2 \end{pmatrix}, \tag{3.24}$$

where z_{1-3} and $\widetilde{\mathbf{f}}^{1,2}$ are the same as in (3.20) and (3.21). This implies that

$$\Delta_{Euler} := \left(\mathbf{v}_{Euler,R} - \mathbf{v}_{Euler,L} \right)^T \widetilde{\mathbf{f}}_{Euler}(\mathbf{u}_L, \mathbf{u}_R) - (\rho u)_R + (\rho u)_L = 0. \tag{3.25}$$

With these, $\hat{\mathbf{v}}$ and $\widetilde{\mathbf{f}}(\mathbf{u}_L, \mathbf{u}_R)$ can be written as

$$\hat{\mathbf{v}} = \begin{pmatrix} \mathbf{v}^1_{Euler} \\ \mathbf{v}^2_{Euler} \\ \mathbf{v}^3_{Euler} \\ -q\mathbf{v}^3_{Euler} \end{pmatrix} \tag{3.26}$$

and

$$\widetilde{\mathbf{f}}(\mathbf{u}_L,\mathbf{u}_R)=\begin{pmatrix}\widetilde{\mathbf{f}}^1_{Euler}\\ \widetilde{\mathbf{f}}^2_{Euler}\\ \widetilde{\mathbf{f}}^3_{Euler}\\ 0\end{pmatrix}+\begin{pmatrix}0\\0\\q\widetilde{\mathbf{f}}_4\\ \widetilde{\mathbf{f}}_4\end{pmatrix}:=\tilde{\mathbf{f}}_1+\tilde{\mathbf{f}}_2, \tag{3.27}$$

where $\mathbf{v}^i_{Euler}$ and $\widetilde{\mathbf{f}}^i_{Euler}$ are the i-th component of $\mathbf{v}_{Euler}$ and $\widetilde{\mathbf{f}}_{Euler}(\mathbf{u}_L,\mathbf{u}_R)$ respectively. Combining (3.25), (3.26) and (3.27), we compute

$$\begin{aligned}
&(\hat{\mathbf{v}}_R-\hat{\mathbf{v}}_L)^T\widetilde{\mathbf{f}}\,(\mathbf{u}_L,\mathbf{u}_R)-(\rho u)_R+(\rho u)_L\\
&=(\hat{\mathbf{v}}_R-\hat{\mathbf{v}}_L)^T(\tilde{\mathbf{f}}_1+\tilde{\mathbf{f}}_2)-(\rho u)_R+(\rho u)_L\\
&=(\hat{\mathbf{v}}_R-\hat{\mathbf{v}}_L)^T\tilde{\mathbf{f}}_1-(\rho u)_R+(\rho u)_L+(\hat{\mathbf{v}}_R-\hat{\mathbf{v}}_L)^T\tilde{\mathbf{f}}_2\\
&=\Delta_{Euler}+(\hat{\mathbf{v}}_R-\hat{\mathbf{v}}_L)^T\tilde{\mathbf{f}}_2\\
&=0.
\end{aligned} \tag{3.28}$$

This means that (3.21) is entropy preserving for the thermodynamic entropy $\hat{U}$, according to Definition 3.1. □

For the entropy stable flux $\hat{\mathbf{f}}(\cdot,\cdot)$, we take the following HLL (Harten-Lax-van Leer) flux [44]:

$$\widehat{\mathbf{f}}\,(\mathbf{u}_L,\mathbf{u}_R)=\begin{cases}\mathbf{f}(\mathbf{u}_L), & \lambda_L\geq 0,\\ \mathbf{f}(\mathbf{u}_R), & \lambda_R\leq 0,\\ \frac{\lambda_R\mathbf{f}_L-\lambda_L\mathbf{f}_R+\lambda_L\lambda_R(\mathbf{u}_R-\mathbf{u}_L)}{\lambda_R-\lambda_L}, & \lambda_L<0<\lambda_R,\end{cases} \tag{3.29}$$

where λ_L,λ_R are some approximations of the leftmost wave speed and the rightmost wave speed, respectively. To determine λ_L,λ_R, we first consider the Riemann problem for the Euler equations without chemical reactions and denote $\hat{\lambda}_{L,R}$ as the approximations of the leftmost and rightmost wave speed proposed in [19], respectively. Those approximations guarantee that $\hat{\lambda}_L$ is not larger than the true leftmost wave speed and $\hat{\lambda}_R$ is not smaller than the true rightmost wave speed [19]. Then we take λ_L,λ_R such that

$$\lambda_L\leq\hat{\lambda}_L<\hat{\lambda}_R\leq\lambda_R \tag{3.30}$$

and obtain

Lemma 3.2. *Under the condition* (3.30)*, the HLL flux* (3.29) *is entropy stable for both the the mathematical entropy U and the thermodynamic entropy $\hat{U}$.*

Proof. Consider the HLL flux for the Euler equations with approximate wave speeds λ_L and λ_R:

$$\widehat{\mathbf{f}}_{Euler}\left(\mathbf{u}_{Euler,L},\mathbf{u}_{Euler,R}\right)=\begin{cases}\mathbf{f}_{Euler}(\mathbf{u}_{Euler,L}), & \lambda_L\geq 0,\\ \mathbf{f}_{Euler}(\mathbf{u}_{Euler,R}), & \lambda_R\leq 0,\\ \frac{\lambda_R\mathbf{u}_{Euler,L}-\lambda_L\mathbf{u}_{Euler,R}+\lambda_L\lambda_R\left(\mathbf{u}_{Euler,R}-\mathbf{u}_{Euler,L}\right)}{\lambda_R-\lambda_L}, & \lambda_L<0<\lambda_R.\end{cases} \tag{3.31}$$

Denote

$$\Delta_{Euler,HLL}:=\left(\mathbf{v}_{Euler,R}-\mathbf{v}_{Euler,L}\right)^T\widehat{\mathbf{f}}_{Euler}\left(\mathbf{u}_{Euler,L},\mathbf{u}_{Euler,R}\right)-(\rho u)_R+(\rho u)_L.$$

Since $\lambda_L\leq\hat{\lambda}_L$ and $\lambda_R\geq\hat{\lambda}_R$, according to Corollary 3.2 of [19], the HLL flux (3.31) for the Euler equations is entropy stable, *i.e.*, $\Delta_{Euler,HLL}\leq 0$. Moreover, we show in Appendix A that

$$\Delta_{T,HLL}:=\left(\hat{\mathbf{v}}_R-\hat{\mathbf{v}}_L\right)^T\widehat{\mathbf{f}}\left(\mathbf{u}_L,\mathbf{u}_R\right)-(\rho u)_R+(\rho u)_L=\Delta_{Euler,HLL} \tag{3.32}$$

and

$$\begin{aligned}\Delta_{M,HLL}&:=\left(\mathbf{v}_R-\mathbf{v}_L\right)^T\widehat{\mathbf{f}}\left(\mathbf{u}_L,\mathbf{u}_R\right)-(\rho u)_R+(\rho u)_L\\&=\Delta_{Euler,HLL}+\frac{(Y_L-Y_R)^2}{\lambda_R^+-\lambda_L^-}[\lambda_R^+\rho_L(\lambda_L^--u_L)+\lambda_L^-\rho_R(\lambda_R^+-u_R)],\end{aligned} \tag{3.33}$$

where $\lambda_R^+=\max(\lambda_R,0)$ and $\lambda_L^-=\min(\lambda_L,0)$. Thus $\Delta_{T,HLL}\leq 0$ and the HLL flux (3.29) is entropy stable for the thermodynamic entropy $\hat{U}$. Furthermore, note that $\hat{\lambda}_L\leq u_L$ and $\hat{\lambda}_R\geq u_R$, we have $\lambda_L^--u_L\leq 0$ and $\lambda_R^+-u_R\geq 0$, and thereby

$$\frac{(Y_L-Y_R)^2}{\lambda_R^+-\lambda_L^-}[\lambda_R^+\rho_L(\lambda_L^--u_L)+\lambda_L^-\rho_R(\lambda_R^+-u_R)]\leq 0.$$

This and (3.33) yield $\Delta_{M,HLL}\leq 0$. Namely, the HLL flux (3.29) is entropy stable for the mathematical entropy U. □

Remark 3.1. *Note that the Lax-Friedrichs flux is a special case of the HLL flux* (3.29) *with* $\lambda_L = -\lambda_R$. *Thus if condition* (3.30) *is satisfied for the Lax-Friedrichs flux, conclusions of Lemma 3.2 also hold.*

With the above two lemmas, we have the following theorem, the proof of which is the same as that of Theorem 3.3 and 3.4 in [19].

Theorem 3.1. *Suppose the boundary is periodic or compatly suported. If* λ_L, λ_R *in the HLL flux* (3.29) *satisfy* (3.30)*, then the scheme* (3.18) *is entropy stable for both thermodynamic entropy* $\hat{U}$ *and mathematical entropy* U*, i.e.,*

$$\frac{d}{dt}\left(\sum_{i=1}^{N}\sum_{j=0}^{k}\frac{\Delta x_i}{2}\omega_j U_j^i\right) \leq \sum_{i=1}^{N}\sum_{j=0}^{k}\frac{\Delta x_i}{2}\omega_j(q\frac{\rho_j^i}{p_j^i}+2Y_j^i)Q_j^i \tag{3.34}$$

and

$$\frac{d}{dt}\left(\sum_{i=1}^{N}\sum_{j=0}^{k}\frac{\Delta x_i}{2}\omega_j \hat{U}_j^i\right) \leq \sum_{i=1}^{N}\sum_{j=0}^{k}\frac{\Delta x_i}{2}\omega_j q\frac{\rho_j^i}{p_j^i}Q_j^i. \tag{3.35}$$

Remark 3.2. *For solid wall boundary condition, one can employ the mirror reflective technique for boundary treatment, which does not destroy the entropy stability of the HLL flux* (3.29)*; See Theorem 4.4 in [19].*

Remark 3.3. *According to [19], the local truncation error of the scheme* (3.18) *is* k*-th order.*

Remark 3.4. *It is worth noting that in the process of constructing our scheme and proving relevant theorems, we only use* $Q \leq 0$ *and do not use the specific form of* Q*. It means that our scheme can be applied to reactive Euler equations with other nonpositive source term.*

3.3. Oscillation-free entropy stable DG scheme

It is well known that DG schemes usually cause spurious oscillations for problems containing discontinuities. Though the DG scheme (3.18) is entropy stable, it cannot eliminate the

spurious oscillation either [19]. To address this issue without destroying the entropy stability, we follow [25] to add a damping term to the scheme (3.18):

$$\frac{\Delta x_i}{2}\frac{d\mathbf{u}_j^i}{dt}+2\sum_{l=0}^{k}D_{jl}\widetilde{\mathbf{f}}\left(\mathbf{u}_j^i,\mathbf{u}_l^i\right)=\frac{\tau_j}{\omega_j}(\mathbf{f}_j^i-\mathbf{f}_{*,j}^i)+\frac{\Delta x_i}{2}\mathbf{s}_j^i-\sigma_i(\mathbf{u})\left(\mathbf{u}_j^i-\sum_{r=0}^{k}\frac{\omega_r}{2}\mathbf{u}_r^i\right), \tag{3.36}$$

where the coefficient $\sigma_i(\mathbf{u})$ is given by

$$\sigma_i(\mathbf{u})=\frac{1}{\Delta x_i}\left[\sum_{l=0}^{1}\frac{h^l}{l+1}\sum_{d=0}^{1}(\max_{1\le s\le 4}(\llbracket\mathbf{L}\partial_x^l\mathbf{u}^s\rrbracket_{i+d-\frac{1}{2}})^2)^{\frac{1}{2}}\right], \tag{3.37}$$

$h=\max_i(\Delta x_i)$, $\mathbf{u}^s$ is the s-th component of the numerical solution $\mathbf{u}$, $\mathbf{L}$ is derived from the characteristic decomposition $\mathbf{f}'(\bar{\mathbf{u}}_{i+\frac{1}{2}})=\mathbf{L}^{-1}\Lambda\mathbf{L}$ with $\bar{\mathbf{u}}_{i+\frac{1}{2}}=\frac{1}{2}(\mathbf{u}_i+\mathbf{u}_{i+1})$. Specifically, $\mathbf{L}$ is taken as [42]

$$\mathbf{L}=\begin{pmatrix} 1-\frac{\gamma-1}{2}\frac{u^2}{c^2} & (\gamma-1)\frac{u}{c^2} & \frac{1-\gamma}{c^2} & q\frac{\gamma-1}{c^2}\\ -\frac{\gamma-1}{2}\frac{u^2}{c^2}Y & (\gamma-1)\frac{u}{c^2}Y & \frac{1-\gamma}{c^2}Y & 1+q\frac{\gamma-1}{c^2}\\ \frac{\gamma-1}{4}\frac{u^2}{c^2}-\frac{u}{2c} & -\frac{\gamma-1}{2}\frac{u}{c^2}+\frac{1}{2c} & \frac{\gamma-1}{2c^2} & q\frac{1-\gamma}{2c^2}\\ \frac{\gamma-1}{4}\frac{u^2}{c^2}+\frac{u}{2c} & -\frac{\gamma-1}{2}\frac{u}{c^2}-\frac{1}{2c} & \frac{\gamma-1}{2c^2} & q\frac{1-\gamma}{2c^2}\end{pmatrix} \tag{3.38}$$

with $c=\sqrt{\frac{\gamma p}{\rho}}$.

Note that this damping term is actually the difference between the solution $\mathbf{u}_j^i$ and its weighted average in the element $\sum_{r=0}^{k}\frac{\omega_r}{2}\mathbf{u}_r^i$.

Thanks to the damping term, the scheme (3.36) can eliminate spurious oscillations for discontinuous problems. It also has many other good properties, such as conservation and high convergence order. Moreover, the scheme still satisfies the entropy stability in Theorem 3.1; see [25] for more details. Additionally, since the average of damping term in one cell is zero [25], the scheme is compatible with positivity-preserving limiters [25]. Based on this, we impose positivity-preserving limiters to the scheme (3.36) in the next section.

4. Positivity preserving limiter for entropy stable schemes

In this section we further consider the positivity of the fully discrete scheme, *i.e.*, the time-discretized version of the scheme (3.36). The entropy stability developed in Section 3

is based on the assumption (3.3) for the positivity of numerical solutions. In this section, we strictly guarantee this positivity assumption for numerical solutions of the scheme (3.36) by adapting the positivity preserving limiter in [24, 9] for the Lax-Fridrichs flux to the HLL flux (3.29). Here we list the main results for the Euler forward method and the proofs are given in Appendix B. High order time stepping methods are discussed in the end of this section.

Lemma 4.1. *Consider the following first order finite volume scheme for* (2.1) *with* $\mathbf{s}(\mathbf{u}) = 0$*:*

$$\mathbf{u}_i^{n+1} = \mathbf{u}_i^n - \lambda[\hat{\mathbf{f}}(\mathbf{u}_i^n, \mathbf{u}_{i+1}^n) - \hat{\mathbf{f}}(\mathbf{u}_{i-1}^n, \mathbf{u}_i^n)], \tag{4.1}$$

where n *refers to the time level,* $\lambda = \frac{\Delta t}{\Delta x}$ *and* $\hat{\mathbf{f}}(\cdot,\cdot)$ *is the HLL flux* (3.29)*. Assume the wave speeds* λ_L, λ_R *in the HLL flux satisfy*

$$\lambda_L \le \min(u_L - c_L, u_R - c_R) < \max(u_L + c_L, u_R + c_R) \le \lambda_R. \tag{4.2}$$

If $\mathbf{u}_j^n \in G$ *for all* j*, then* $\mathbf{u}_i^{n+1} \in G$ *under the CFL condition* $\lambda a_0 \le \frac{1}{2}$ *with* $a_0 = \||u| + c\|_\infty$*.*

Lemma 4.2. *Consider the scheme satisfied by the cell average of the DG scheme* (3.36) *for* (2.1) *with* $\mathbf{s}(\mathbf{u}) = 0$*:*

$$\bar{\mathbf{u}}^{i,n+1} = \bar{\mathbf{u}}^{i,n} - \lambda \left[\hat{\mathbf{f}}(\mathbf{u}_{i+1/2}^-, \mathbf{u}_{i+1/2}^+) - \hat{\mathbf{f}}(\mathbf{u}_{i-1/2}^-, \mathbf{u}_{i-1/2}^+)\right], \tag{4.3}$$

where $\bar{\mathbf{u}}^{i,n} = \sum_{j=0}^k \frac{\omega_j}{2} \mathbf{u}_j^{i,n}$ *is the cell average of* $\mathbf{u}$ *on* I_i *at time level* n*,* $\hat{\mathbf{f}}(\cdot,\cdot)$ *is the HLL flux* (3.29) *with wave speeds satisfying* (4.2)*, and* $\mathbf{u}_{i+1/2}^-, \mathbf{u}_{i+1/2}^+$ *are the approximations of the point values* $\mathbf{u}(x_{i+1/2}, t_n)$ *within the cells* I_i *and* I_{i+1}*, respectively. If* $\mathbf{u}_j^{i,n}$ *and* $\bar{\mathbf{u}}^{i,n} \in G$ *for all* j*, then* $\bar{\mathbf{u}}^{i,n+1} \in G$ *under the CFL condition* $\lambda a_0 \le \frac{1}{4}\omega_0$*.*

Theorem 4.1. *Consider the scheme satisfied by the cell average of the DG scheme* (3.36) *for* (2.1)*:*

$$\bar{\mathbf{u}}^{i,n+1} = \bar{\mathbf{u}}^{i,n} - \lambda \left[\hat{\mathbf{f}}(\mathbf{u}_{i+1/2}^-, \mathbf{u}_{i+1/2}^+) - \hat{\mathbf{f}}(\mathbf{u}_{i-1/2}^-, \mathbf{u}_{i-1/2}^+)\right] + \Delta t \bar{\mathbf{s}}^{i,n}, \tag{4.4}$$

where $\bar{\mathbf{s}}^{i,n} = \sum_{j=0}^{k} \frac{\omega_j}{2} \mathbf{s}_j^{i,n}$ *is the cell average of* $\mathbf{s}(\mathbf{u})$ *on* I_i *at time level* n. *If* $\mathbf{u}_j^{i,n}$ *and* $\bar{\mathbf{u}}^{i,n} \in G$ *for all* j, *then* $\bar{\mathbf{u}}^{i,n+1} \in G$ *under the CFL condition* $\lambda a_0 \leq \frac{1}{8}\omega_0$ *and* $\max_{i,j}\{\Delta t \tilde{K} e^{-\tilde{T}/T_j^{i,n}}\} \leq \frac{1}{2}$.

Based on Theorem 4.1, we follow [24, 9] to implement positivity preserving limiters for the fully discrete (time-discretized) version of the scheme (3.36) to guarantee the positivity condition (3.3). The main idea is to modify the distribution of some variables in each cell to make its value at the quadrature nodes positive, while keeping the cell average unchanged. For convenience of representation, we concentrate on a single cell I_i at time level n and omit the superscripts i and n. We denote the set consisting of quadrature nodes in I_i as S, the DG polynomial in I_i as $\mathbf{u}(x) = (\rho(x), \rho u(x), \rho E(x), \rho Y(x))^T$, the cell average of $\mathbf{u}(x)$ in I_i as $\bar{\mathbf{u}} = \left(\bar{\rho}, \overline{\rho u}, \overline{\rho E}, \overline{\rho Y}\right)^T$, and the modified DG polynomial in I_i as $\widehat{\mathbf{u}}(x) = \left(\widehat{\rho}(x), \widehat{\rho u}(x), \widehat{\rho E}(x), \widehat{\rho Y}(x)\right)^T$. Then for each cell I_i we implement the following algorithm to guarantee the positivity of ρ, p, Y at the quadrature nodes as in [9].

1. Pick a small number ε such that $\varepsilon \leq \min_i\{\bar{\rho}_i^n, p(\bar{\mathbf{u}}_i^n)\}$, where $\bar{\rho}_i^n$ and $\bar{\mathbf{u}}_i^n$ are the cell averages of density ρ and $\mathbf{u}$ in I_i at time level n. In practice, we usually set $\varepsilon = 10^{-13}$.
2. Modify the density ρ. Denote

$$\rho_{min} = \min_{x \in S} \rho(x)$$

   If $\rho_{min} < \varepsilon$, we take

$$\hat{\rho}(x) = \bar{\rho} + \theta_1(\rho(x) - \bar{\rho}), \quad x \in S$$

   with

$$\theta_1 = \frac{\bar{\rho} - \varepsilon}{\bar{\rho} - \rho_{min}}$$

3. Modify ρY. Denote

$$\rho Y_{min} = \min_{x \in S} \rho Y(x).$$

If $\rho Y_{min} < 0$, we take

$$\widehat{\rho Y}(x) = \overline{\rho Y} + \theta_2(\rho Y(x) - \overline{\rho Y}), \quad x \in S$$

with

$$\theta_2 = \frac{\overline{\rho Y}}{\overline{\rho Y} - \rho Y_{min}}.$$

4. Modify the pressure p. Let $\tilde{\mathbf{u}}(x) = \left(\widehat{\rho}(x), \rho u(x), \rho E(x), \widehat{\rho Y}(x)\right)^T$. Define $\theta = \min_{x\in S} \theta_x$ with

$$\theta_x = \begin{cases} 1, & p(\tilde{\mathbf{u}}(x)) \geq 0, \\ \dfrac{p(\bar{\mathbf{u}})}{p(\bar{\mathbf{u}}) - p(\tilde{\mathbf{u}})}, & \text{otherwise.} \end{cases} \tag{4.5}$$

Then we take

$$\widehat{\mathbf{u}(x)} = \bar{\mathbf{u}} + \theta(\tilde{\mathbf{u}}(x) - \bar{\mathbf{u}}), \quad x \in S.$$

Remark 4.1. *Since the high order SSP RK methods can be written as convex combinations of the Euler forward method, the above positivity preserving limiters can also be applied to these time stepping methods [22]. In doing so, we need to estimate* $\||u| + c\|_\infty$ *and the source term* $\mathbf{s}(\mathbf{u})$ *for all stages accurately at each time step, which is highly nontrivial. In practice, we could multiply factors to* $\||u| + c\|_\infty$ *and* $\mathbf{s}(\mathbf{u})$ *at the first stage as approximations for the intermediate ones. More details can be found in the Remark 2.7 of [22].*

Remark 4.2. *According to Theorem 3.7 of [19], the above positivity preserving limiters do not destroy the entropy stability in Theorem 3.1.*

Remark 4.3. *Combining conditions* (3.30) *and* (4.2)*, the estimations* λ_L *and* λ_R *in HLL flux* (3.29) *can be chosen as*

$$\lambda_L = \min\left\{\hat{\lambda}_L, u_L - c_L, u_R - c_R\right\}, \lambda_R = \max\left\{\hat{\lambda}_R, u_L + c_L, u_R + c_R\right\}. \tag{4.6}$$

5. Time discretization and generalization to 2D cases

5.1. Time discretization

In this subsection we consider the time discretizaiton of the semi-discrete scheme (3.36). For convenience, we write the scheme as

$$\frac{d\mathbf{u}}{dt} = \mathbf{F}(\mathbf{u}) + \mathbf{G}(\mathbf{u}), \tag{5.7}$$

where $\mathbf{F}(\mathbf{u})$ contains the terms related to the convection part and the source term and $\mathbf{G}(\mathbf{u})$ stands for the damping term. Here we consider four kinds of time discretizaitons. The first kind is the following second-order explicit SSP RK method [47]

$$\begin{aligned} \mathbf{u}^{(1)} &= \mathbf{u}^n + \Delta t(\mathbf{F}\left(\mathbf{u}^n\right) + \mathbf{G}\left(\mathbf{u}^n\right)), \\ \mathbf{u}^{n+1} &= \frac{1}{2}\mathbf{u}^n + \frac{1}{2}\mathbf{u}^{(1)} + \frac{1}{2}\Delta t(\mathbf{F}\left(\mathbf{u}^{(1)}\right) + \mathbf{G}\left(\mathbf{u}^{(1)}\right)). \end{aligned} \tag{5.8}$$

This method is used in convergence order tests of our scheme on P^2 elements. The second kind is the following third-order explicit SSP RK method [47]

$$\begin{aligned} \mathbf{u}^{(1)} &= \mathbf{u}^n + \Delta t(\mathbf{F}\left(\mathbf{u}^n\right) + \mathbf{G}\left(\mathbf{u}^n\right)), \\ \mathbf{u}^{(2)} &= \frac{3}{4}\mathbf{u}^n + \frac{1}{4}\mathbf{u}^{(1)} + \frac{1}{4}\Delta t(\mathbf{F}\left(\mathbf{u}^{(1)}\right) + \mathbf{G}\left(\mathbf{u}^{(1)}\right)), \\ \mathbf{u}^{n+1} &= \frac{1}{3}\mathbf{u}^n + \frac{2}{3}\mathbf{u}^{(2)} + \frac{2}{3}\Delta t(\mathbf{F}\left(\mathbf{u}^{(2)}\right) + \mathbf{G}\left(\mathbf{u}^{(2)}\right)). \end{aligned} \tag{5.9}$$

This method is employed for most of our numerical examples, including the convergence order tests of the scheme on P^3 elements. The third kind is the following fourth-order explicit SSP

RK method [48].

$$
\begin{aligned}
\mathbf{u}^{(1)} =& \mathbf{u}^n + 0.391752226571890\Delta t(\mathbf{F}\left(\mathbf{u}^n\right) + \mathbf{G}\left(\mathbf{u}^n\right)) \\
\mathbf{u}^{(2)} =& 0.444370493651235\mathbf{u}^n + 0.555629506348765\mathbf{u}^{(1)} + 0.368410593050371\Delta t(\mathbf{F}\left(\mathbf{u}^{(1)}\right) + \mathbf{G}\left(\mathbf{u}^{(1)}\right)), \\
\mathbf{u}^{(3)} =& 0.620101851488403\mathbf{u}^n + 0.379898148511597\mathbf{u}^{(2)} + 0.251891774271694\Delta t(\mathbf{F}\left(\mathbf{u}^{(2)}\right) + \mathbf{G}\left(\mathbf{u}^{(2)}\right)), \\
\mathbf{u}^{(4)} =& 0.178079954393132\mathbf{u}^n + 0.821920045606868\mathbf{u}^{(3)} + 0.544974750228521\Delta t(\mathbf{F}\left(\mathbf{u}^{(3)}\right) + \mathbf{G}\left(\mathbf{u}^{(3)}\right)), \\
\mathbf{u}^{n+1} =& 0.517231671970585\mathbf{u}^{(2)} + 0.096059710526147\mathbf{u}^{(3)} + 0.063692468666290\Delta t(\mathbf{F}\left(\mathbf{u}^{(3)}\right) + \mathbf{G}\left(\mathbf{u}^{(3)}\right)) \\
& + 0.386708617503268\mathbf{u}^{(4)} + 0.226007483236906\Delta t(\mathbf{F}\left(\mathbf{u}^{(4)}\right) + \mathbf{G}\left(\mathbf{u}^{(4)}\right)).
\end{aligned} \tag{5.10}
$$

It is used in convergence order tests of the scheme on P^4 elements.

For some tough problems, the damping term may be quite large, leading to a very restrictive time step for the above method. In this case, we use the following second-order exponential RK method [49]

$$
\begin{aligned}
\mathbf{u}^{(1)} &= e^{-\mu\Delta t}\left(\left(\mathbf{u}^n + \Delta t\mathbf{F}\left(\mathbf{u}^n\right)\right) + \Delta t\left(\mathbf{G}\left(\mathbf{u}^n\right) + \mu\mathbf{u}^n\right)\right), \\
\mathbf{u}^{n+1} &= \frac{1}{2}e^{-\mu\Delta t}\mathbf{u}^n + \frac{1}{2}\left(\left(\mathbf{u}^{(1)} + \Delta t\mathbf{F}\left(\mathbf{u}^{(1)}\right)\right) + \Delta t\left(\mathbf{G}\left(\mathbf{u}^{(1)}\right) + \mu\mathbf{u}^{(1)}\right)\right),
\end{aligned} \tag{5.11}
$$

where μ is a constant. When $\mu\Delta t$ is large, $e^{-\mu\Delta t}$ will be very small and leads to a wrong numerical solution. This can be improved by replacing $e^{-\mu\Delta t}$ with $1/(1+\mu\Delta t+\frac{1}{2}(\mu\Delta t)^2)$ [49], which has been adopted in our simulations. Here we mention that high order exponential RK methods for time discretization of stiff problems can be found in [50, 51, 30].

Since the four methods are all SSP, the positivity preserving limiters can be imposed as in Remark 4.1. Considering the condition for the positivity in Theorem 4.1 and the CFL condition, we take Δt as

$$
\Delta t = \min\left\{CFL\frac{h}{a_0}, \quad \frac{\omega_0}{8aa_0}h, \quad \frac{1}{2b\tilde{K}}\min_{i,j} e^{\tilde{T}/T_j^{i,n}}\right\} \tag{5.12}
$$

for discontinuous problems, where $h = \max_i\left(\Delta x_i\right)$, CFL is CFL number and a and b are proper factors mentioned in Remark 4.1. For accuracy test, we set $\Delta t = O(\Delta x)$.

5.2. Generalization to 2D cases

Though the scheme (3.36) is designed for 1D reactive Euler equations, it can be straightforwardly extended to 2D cases on rectangle meshes. Here we list the main idea. First, using tensor product for (3.18), we obtain nodal entropy stable for 2D reactive Euler equations on rectangular meshes. Then we add the damping terms in [25] to the nodal entropy stable DG scheme to make it oscillation-free, which is derived on simplex meshes consisting of rectangular meshes originally. Finally, we slightly adapt the positivity preserving limiter in Section 4 to the 2D oscillation-free entropy stable scheme. In this way, we obtain the positivity preserving and oscillation-free entropy stable DG scheme on rectangle meshes.

Our scheme can also be generalized to 2D cases on unstructured meshes with general nodes. The key idea is to construct entropy stable DG scheme on these meshes by multi-dimensional SBP matrices and then apply corresponding positivity preserving limiters and damping terms to the DG scheme. Here we briefly introduce three approaches to construct matrices with SBP properties. The first one is proposed in [19] by using a special Gauss-Lobatto type quadrature with collocated surface quadrature points. The second one is to treat volume nodes and surfaces nodes in one element as a whole and the resulting matrices are called hybridized SBP matrices [32, 31]. The third one is to combine the values on all nodes in different elements as a group vector to obtain global SBP matrices [33, 34].

6. Numerical examples

In this section, we validate the oscillation-free entropy stable DG scheme (3.36) with positivity preserving limiters via various 1D and 2D examples, most of which are from [22, 19, 9]. We test the convergence order of the scheme on P^k elements with $k = 2, 3, 4$ through examples with smooth solutions. In these examples, the SSP RK schemes (5.8),(5.9),(5.10)

are employed as time discretizations for P^k elements with $k = 2, 3, 4$, respectively. Schemes on P^3 and P^2 elements are employed for 1D and 2D examples with discontinuities, respectively. The third-order SSP RK method (5.9) and the second-order exponential RK method (5.11) with time step (5.12) are employed for non-stiff and stiff discontinuous problems, respectively. The approximations of wave speeds λ_L and λ_R in HLL flux are determined by (4.6). Except for Fig. 6.1 ((d)-(f)), the values plotted in the figures for 1D examples are cell averages of solutions within each cell. For contour plots in 2D examples, we adopt the values of the numerical solution at Gauss-Lobatto points to achieve better resolution.

6.1. 1D examples

Example 1. We first verify the accuracy of our scheme via a 1D example with analytical solution

$$\rho(x,t) = 1 - 0.99\sin(x-t), \quad u(x,t) = 1, \quad p(x,t) = 0.01, \quad Y(x,t) = 0,$$

which is adapted from [22]. The computational domain is $[0, 2\pi]$ and the boundary is periodic. As mentioned before, the SSP RK schemes (5.8),(5.9),(5.10) are employed as time discretizations for P^k elements with $k = 2, 3, 4$, respectively. The time step is taken as $\Delta t = 0.1\Delta x$. The errors at $t = 0.02$ and the convergence orders are listed in Table 6.1. It can be observed that the convergence orders in this example are one order higher than the designed ones. This phenomenon was also reported in [19] and a possible reason is that Gauss-Lobatto quadrature is exact for linear convective part.

Example 2. In this example, we further test the convergence order of our scheme for $Y \neq 0$. As in the previous example, the computational domain is $[0, 2\pi]$ and the boundary is periodic. The only difference is that the initial data is changed to be

$$\rho(x,0) = 1 - 0.99\sin(x), \quad u(x,0) = 1, \quad p(x,0) = 0.01, \quad Y(x,0) = 0.5 + 0.49\sin(x).$$

Table 6.1: Error table for the 1D smooth problem with $Y = 0$.

			$k = 2$			
Δx	l^1 error	order	l^2 error	order	l^∞ error	order
$\pi/32$	7.41e-06		1.32e-05		9.05e-05	
$\pi/64$	1.39e-06	2.41	2.81e-06	2.23	2.13e-05	2.09
$\pi/128$	1.78e-07	2.96	4.08e-07	2.78	3.16e-06	2.75
$\pi/256$	2.07e-08	3.11	4.74e-08	3.10	3.65e-07	3.11
			$k = 3$			
Δx	l^1 error	order	l^2 error	order	l^∞ error	order
$\pi/32$	2.27e-07		8.23e-07		6.82e-06	
$\pi/64$	2.40e-08	3.24	1.03e-07	3.00	1.40e-06	2.28
$\pi/128$	1.35e-09	4.15	7.23e-09	3.83	1.14e-07	3.63
$\pi/256$	8.71e-11	3.96	4.21e-10	4.10	6.60e-09	4.15
			$k = 4$			
Δx	l^1 error	order	l^2 error	order	l^∞ error	order
$\pi/16$	4.04e-07		1.48e-06		1.20e-05	
$\pi/32$	2.85e-08	3.83	1.50e-07	3.31	1.67e-06	2.84
$\pi/64$	9.35e-10	4.93	5.20e-09	4.85	7.05e-08	4.57
$\pi/128$	2.97e-11	4.98	1.93e-10	4.75	3.02e-09	4.55

In this case, the analytical solutions are unavailable and we use results obtained with our scheme on P^4 elements with $\Delta x = \pi/512$ as reference solutions. With the same time discretizations in Example 1, the errors at $t = 0.02$ are given in Table 6.2. The convergence behavior of the scheme is similar to that in Example 1 and it can be observed again that the convergence orders are one order higher than the designed ones.

Example 3. Next we consider Sod's shock tube problem with initial data [52]

$$(\rho, w, p, Y) = \begin{cases} (1, 0, 1, 0), & x < 0, \\ (0.125, 0, 0.1, 0), & x \geq 0. \end{cases}$$

The computational domain is $[-1, 1]$ and the terminal time is $t = 0.1$. In this problem, the mathematical entropy is the same as the thermodynamic entropy as $Y \equiv 0$. CFL number is taken as 0.2. The density, velocity and pressure and total entropy with $\Delta x = \frac{1}{120}$ are plotted in Fig. 6.1. It can be seen that the cell averages of numerical solutions are free of oscillations

Table 6.2: Error table for the 1D smooth problem with $Y \neq 0$.

			$k=2$			
Δx	l^1 error	order	l^2 error	order	l^∞ error	order
$\pi/32$	7.24e-06		1.31e-05		9.05e-05	
$\pi/64$	1.38e-06	2.40	2.81e-06	2.23	2.13e-05	2.09
$\pi/128$	1.77e-07	2.96	4.08e-07	2.78	3.16e-06	2.75
$\pi/256$	2.07e-08	3.10	4.74e-08	3.10	3.65e-07	3.11
			$k=3$			
Δx	l^1 error	order	l^2 error	order	l^∞ error	order
$\pi/32$	2.26e-07		8.23e-07		6.82e-06	
$\pi/64$	2.40e-08	3.24	1.03e-07	3.00	1.40e-06	2.28
$\pi/128$	1.35e-09	4.15	7.23e-09	3.83	1.14e-07	3.62
$\pi/256$	8.72e-11	3.95	4.21e-10	4.10	6.41e-09	4.15
			$k=4$			
Δx	l^1 error	order	l^2 error	order	l^∞ error	order
$\pi/16$	3.56e-07		1.44e-06		1.20e-05	
$\pi/32$	2.77e-08	3.69	1.49e-07	3.27	1.67e-06	2.84
$\pi/64$	8.78e-10	4.98	5.18e-09	4.85	7.05e-08	4.57
$\pi/128$	2.71e-11	5.02	1.91e-10	4.76	3.01e-09	4.55

and agree well with the exact ones. Additionally, the total entropy decreases in time as expected. However, for the polynomial solutions, there are some spurious oscillations. Such phenomenon was also reported in [27] for the results of the oscillation-free DG schemes. To address this issue, a novel damping term has been recently proposed in [53], with which the polynomial solutions are also free of oscillations.

Example 4. In this example we simulate the double rarefaction problem [54]. The initial condition for this problem is

$$(\rho, w, p, Y) = \begin{cases} (7, -1, 0.2, 0), & x < 0, \\ (7, 1, 0.2, 0), & x \geq 0. \end{cases}$$

The computational domain is $[-1, 1]$ and the terminal time is $t = 0.6$. The exact solution of this problem contains vacuum and thus the positivity-preserving property of our scheme is essential.

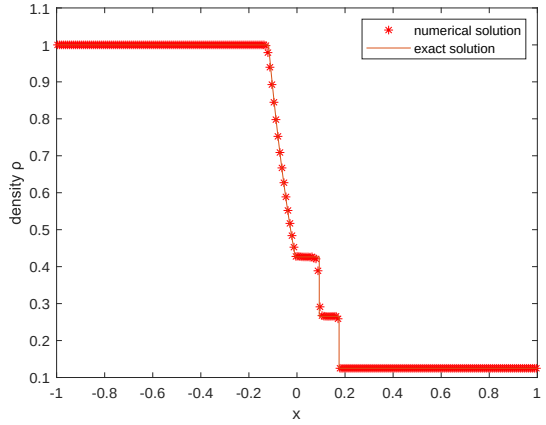

(a) Cell averages of density

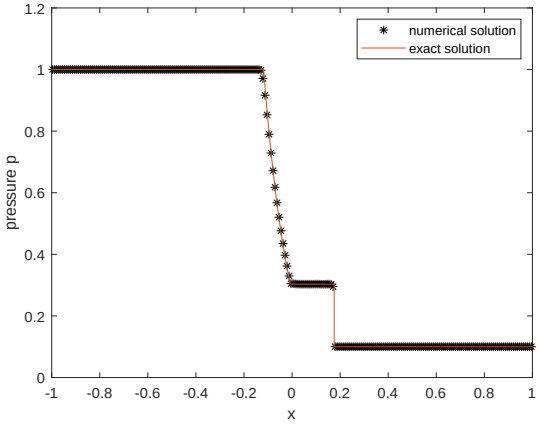

(b) Cell averages of pressure

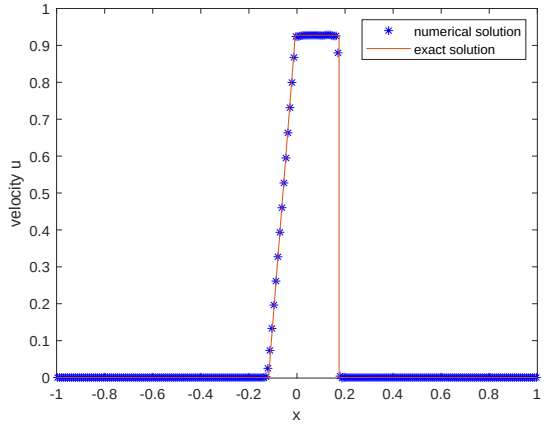

(c) Cell averages of velocity

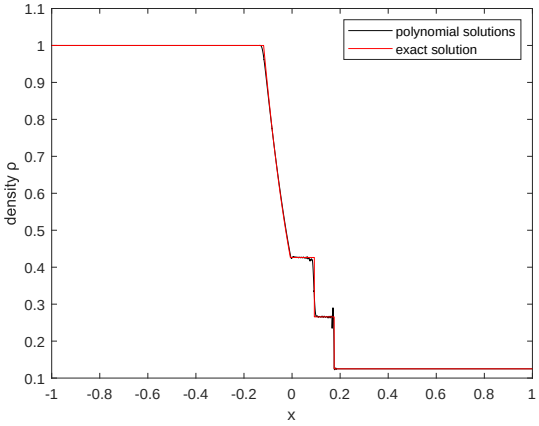

(d) Polynomial solutions of density

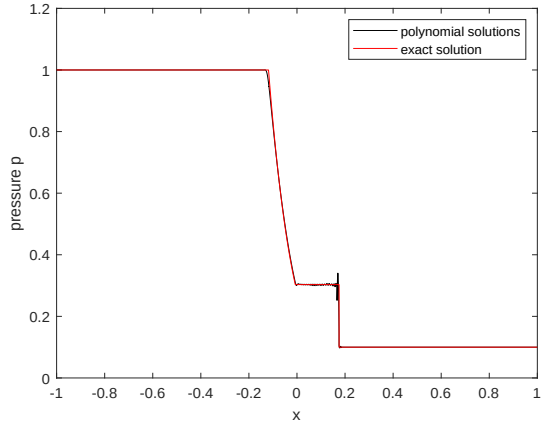

(e) Polynomial solutions of pressure

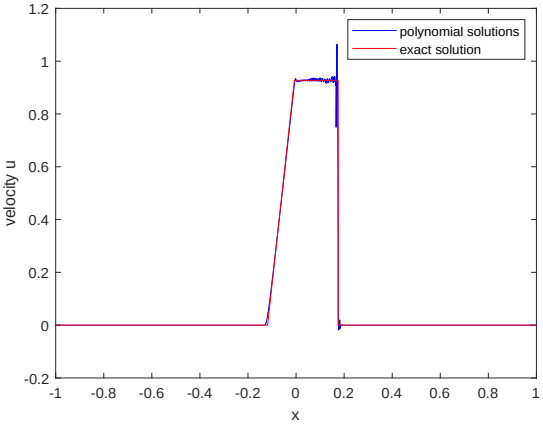

(f) Polynomial solutions of velocity

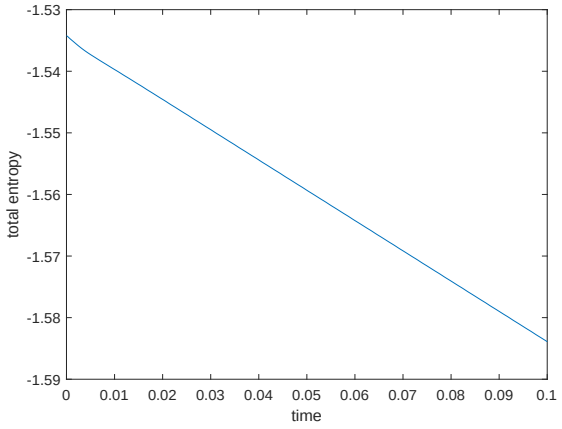

(g) Total entropy with time

Figure 6.1: Example 3: Solutions at $t = 0.1$ with $\Delta x = \frac{1}{120}$ and the evaluation of the total entropy for Sod's shock tube problem.

The numerical solutions with $\Delta x = \frac{1}{240}$ and CFL=0.2 are given in Fig. 6.2, from which we can observe that the low density and low pressure are both captured very well. Besides, it is also clear that the total entropy decreases with time evolving.

Example 5. We further simulate the steady denotation problem, which has been widely studied; see *e.g.* [55, 8, 7]. The initial condition is

$$(\rho, u, p, Y) = \begin{cases} (2.5706, 6.86089, 80.02055, 0), & x \leqslant 2, \\ (1, 0, 1, 1), & x > 2 \end{cases}$$

and the computational domain is $[0, 100]$. CFL number is taken as 0.1. The comparison of numerical solutions at $t = 7.5$ with $\Delta x = 1/15$ and the reference solution from [55] are provided in Fig. 6.3. Clearly, the classical ZND structure is resolved very well. Fig. 6.3 also shows the decrease of both the mathematical entropy and the thermodynamic entropy, which validated the entropy stability of the scheme for both entropies.

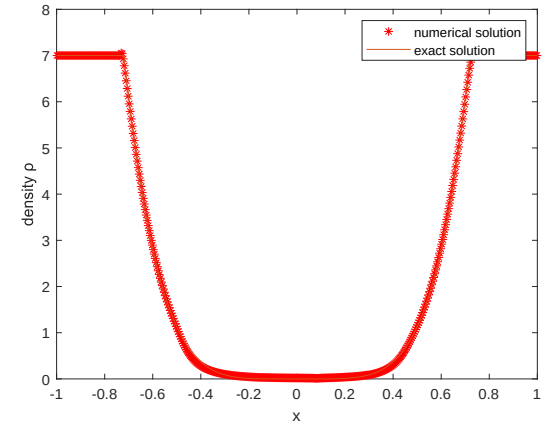

(a) Density

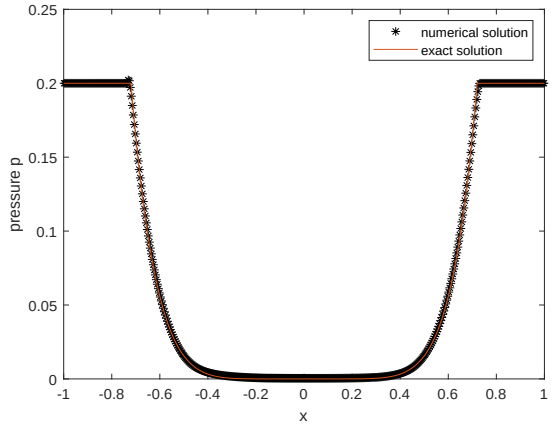

(b) Pressure

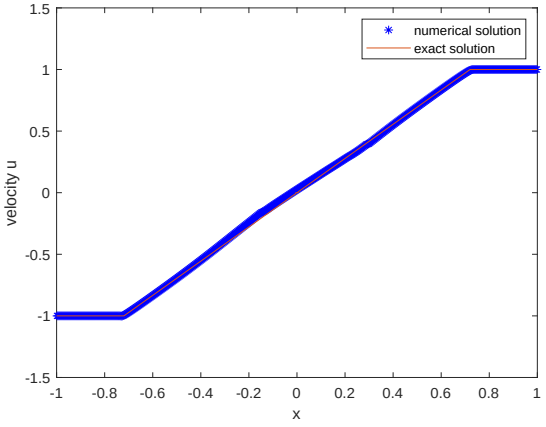

(c) Velocity

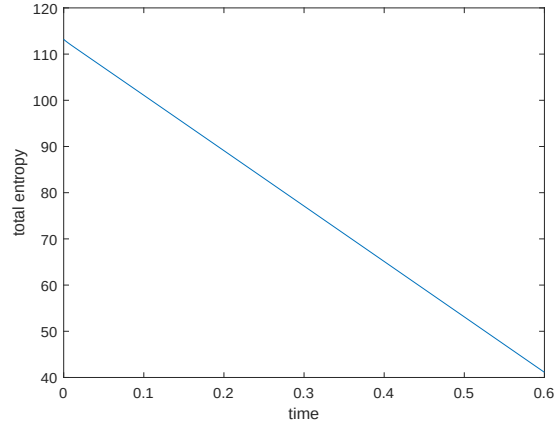

(d) Total entropy with time

Figure 6.2: Example 4: Solutions at $t = 0.6$ with $\Delta x = \frac{1}{240}$ and the evaluation of the total entropy for the double rarefaction problem.

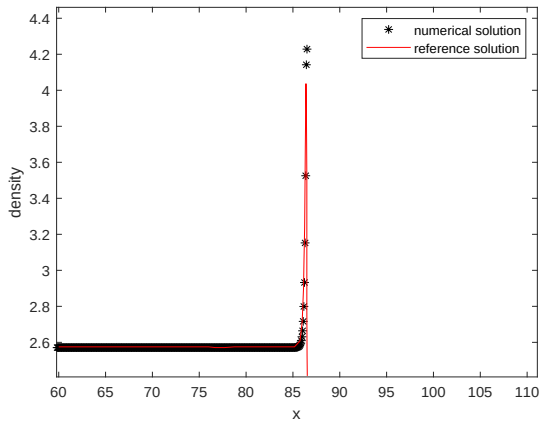

(a) Density

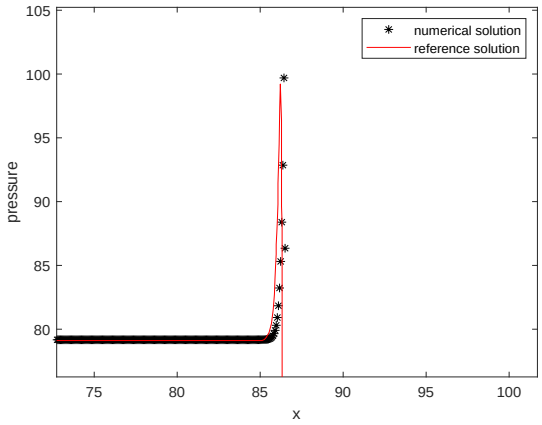

(b) Pressure

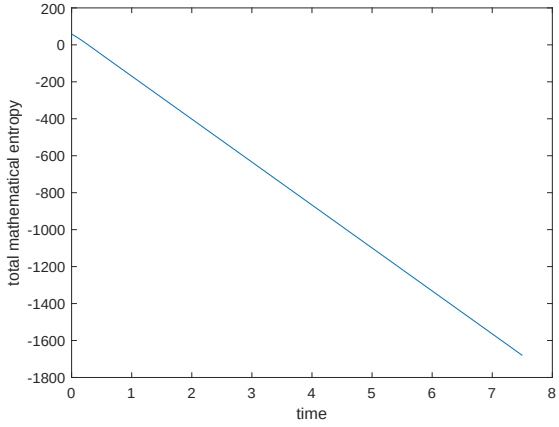

(c) Total mathematical entropy with time

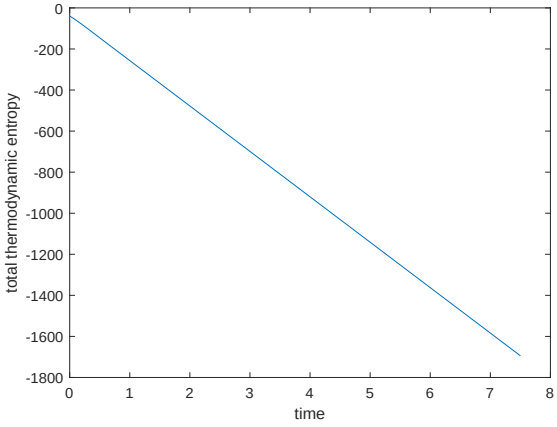

(d) Total thermodynamic entropy with time

Figure 6.3: Example 5: Solutions at $t = 7.5$ with $\Delta x = \frac{1}{15}$ and the evaluation of the total entropies for the stable denotation problem.

Example 6. This example is the interaction of two blast waves with initial data [56]

$$\rho = 1, \quad u = 0, \quad Y = 0, \quad p = \begin{cases} 1000, & 0 < x < 0.1, \\ 0.01, & 0.1 < x < 0.9, \\ 100, & 0.9 < x < 1. \end{cases}$$

The computational domain is $[0, 1]$ and the reflective boundary condition is imposed at $x = 0$ and $x = 1$.

This problem involves multiple reflections of shocks and rarefaction waves off the walls. On the one hand, the solutions computed by the traditional DG scheme blow up easily due to negative density or pressure. On the other hand, if we directly use the entropy stable DG scheme only with positivity-preserving limiter to solve the problem, the spurious oscillations will cover the true solution severely. On the contrary, thanks to the positivity preserving limiters and the damping terms, our scheme can preserve the positivity of density and pressure and suppress the oscillations, while keeping the entropy stability. The density profiles at $t = 0.038$ with $\Delta x = 1/500$ and $CFL = 0.1$ and the total entropy evolving with time are given in Fig. 6.4. Obviously, all shocks and structures are resolved correctly without spurious oscillations.

6.2. 2D examples

Example 7. In the following we consider 2D examples. We first test the convergence order with exact solution

$$\rho(x, y, t) = 1 - 0.99 \sin(x + y - 2t), \quad u = 1, \quad v = 1, \quad p = 0.01, \quad Y = 0$$

in the domain $[0, 2\pi]^2$. This solution is adapted from [22] by reducing the density and pressure to validate the positivity preserving limiters simultaneously. We set $\Delta y = \Delta x$ and $\Delta t = 0.1\Delta x$. The errors at terminal time $t = 0.02$ are presented in Table 6.3, from which designed orders of convergence can be observed.

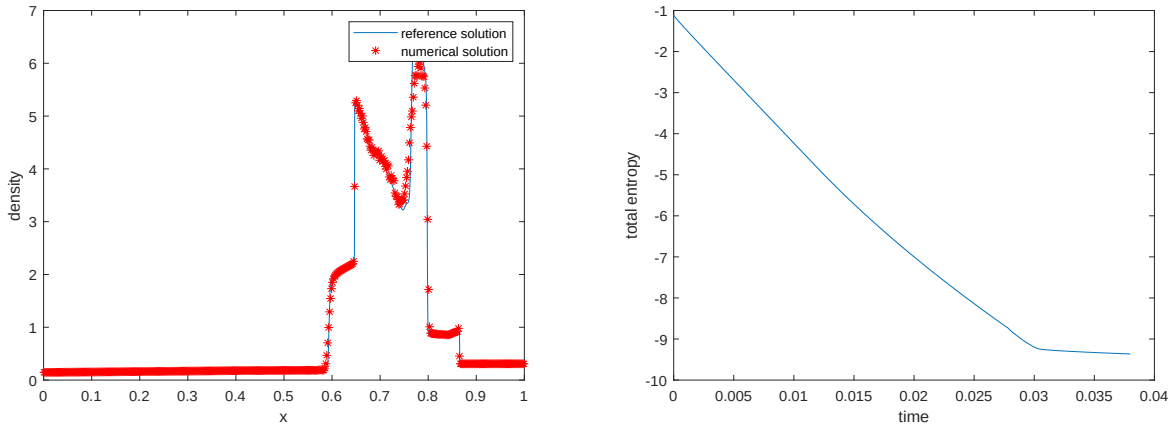

(a) Density (b) Total entropy against time

Figure 6.4: Example 6: Density profiles at $t = 0.038$ with $\Delta x = 1/500$ and the evaluation of the total entropies for the interaction of blast waves.

Table 6.3: Example 7: Error table for the 2D problem with smooth solutions. Here $\Delta y = \Delta x$.

			$k = 2$			
Δx	l^1 error	order	l^2 error	order	l^∞ error	order
$\pi/8$	1.83e-04		3.11e-04		1.60e-03	
$\pi/16$	4.68e-05	1.97	8.42e-05	1.88	6.22e-04	1.36
$\pi/32$	1.10e-05	2.09	2.08e-05	2.02	1.88e-04	1.73
$\pi/64$	2.22e-06	2.30	4.42e-06	2.24	4.08e-05	2.22
			$k = 3$			
Δx	l^1 error	order	l^2 error	order	l^∞ error	order
$\pi/8$	2.83e-05		8.13e-05		5.49e-04	
$\pi/16$	3.56e-06	2.99	1.27e-05	2.68	1.10e-04	2.33
$\pi/32$	3.49e-07	3.35	1.56e-06	3.02	2.48e-05	2.15
$\pi/64$	3.71e-08	3.23	1.57e-07	3.32	2.91e-06	3.09
			$k = 4$			
Δx	l^1 error	order	l^2 error	order	l^∞ error	order
$\pi/8$	9.80e-06		3.16e-05		2.22e-04	
$\pi/16$	6.55e-07	3.90	2.96e-06	3.42	4.33e-05	2.36
$\pi/32$	3.41e-08	4.27	1.67e-07	4.15	2.24e-06	4.27
$\pi/64$	1.41e-09	4.60	7.65e-09	4.45	1.52e-07	3.88

Example 8. Next we simulate the 2D blast waves problem with initial condition [9]

$$(\rho, u, v, p, Y) = \begin{cases} (1, 0, 0, 80, 0), & x^2 + y^2 \leqslant 0.36, \\ (1, 0, 0, 10^{-9}, 1), & x^2 + y^2 > 0.36. \end{cases}$$

The computational domain is $[0, 2]^2$ and there are solid walls at the left and bottom boundaries.

Because the pressure of two initial states differs greatly, the damping term could be very large compared with the other terms. This leads to very restrictive time step if we use explicit SSP RK method for time discretization. As mentioned in Section 5.1, here we adopt the exponential Runge-Kutta method (5.9) instead. The numerical solutions with $\Delta x = \Delta y = 1/60$ and $CFL = 0.5$ at terminal time $t = 0.2$ are shown in Figure 6.5. From the solutions, we can observe our scheme resolve the structures of blast waves successfully without obvious spurious oscillations or entropy increasing.

Example 9. In this example we simulate gaseous detonation waves through a rectangle geometry [9]. The initial condition is

$$(\rho, u, v, p, Y) = \begin{cases} (1, 0, 0, 80, 0), & x < 0.5, \\ (1, 0, 0, 55, 1), & x \geqslant 0.5. \end{cases}$$

The computational domain is $[0, 5] \times [0, 5]$ and the rectangle is located in $[0, 1] \times [0, 2]$. The solid walls are located everywhere except at $x = 0, (\rho, u, v, E, Y) = (11, 6.18, 0, 970, 1)$. This is a challenging problem for numerical simulation because the pressure and density will drop very close to zero near the corner.

The terminal time is $t = 0.6$ and the mesh is uniformly rectangular with $\Delta x = \Delta y = 1/32$. CFL number is taken as 0.65. Fig. 6.6 plots the density and pressure contours and the total entropies against time. We can see the denotation wave structures are resolved very clearly and there are no instability or oscillations.

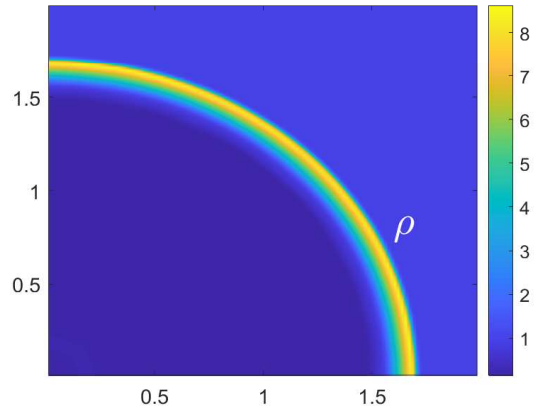

(a) Density

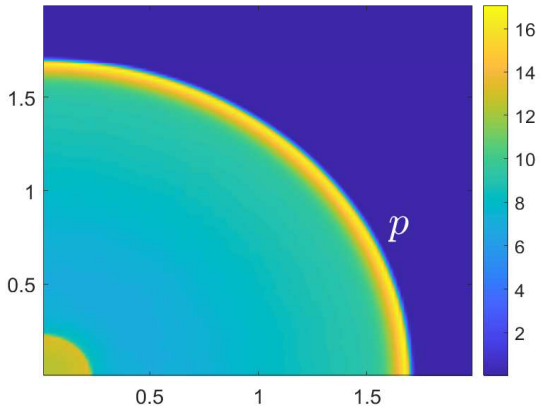

(b) Pressure

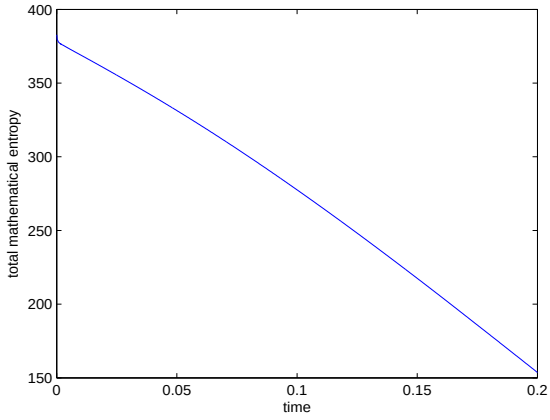

(c) Total mathematical entropy against time

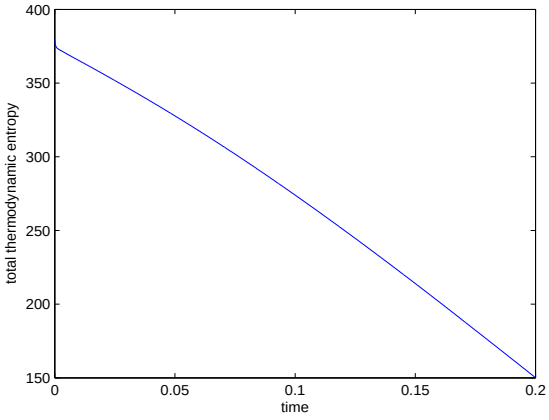

(d) Total thermodynamic entropy against time

Figure 6.5: Example 8: Density and pressure profiles at $t = 0.2$ with $\Delta x = \Delta y = 1/60$ and the evaluation of the total entropies for the 2D blast waves.

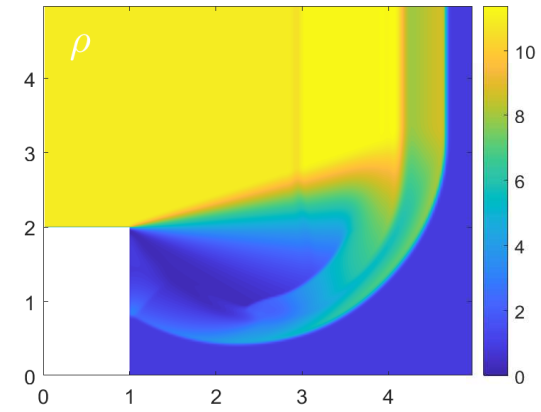

(a) Density

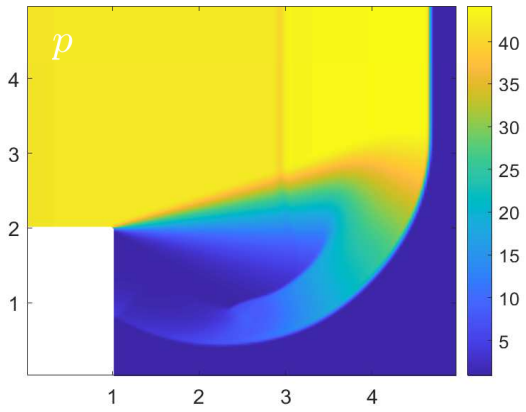

(b) Pressure

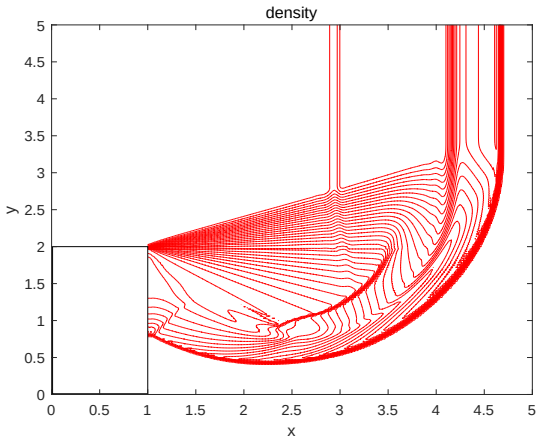

(c) 32 contour lines of density

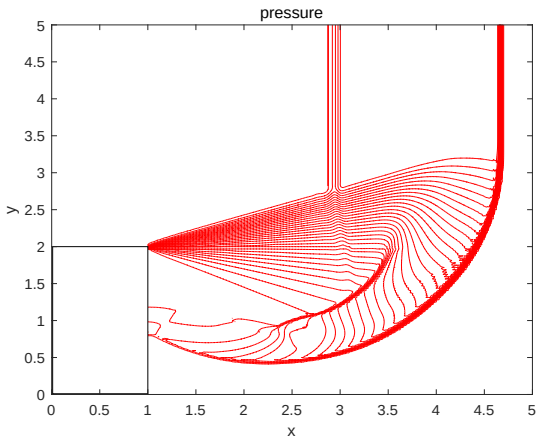

(d) 32 contour lines of pressure

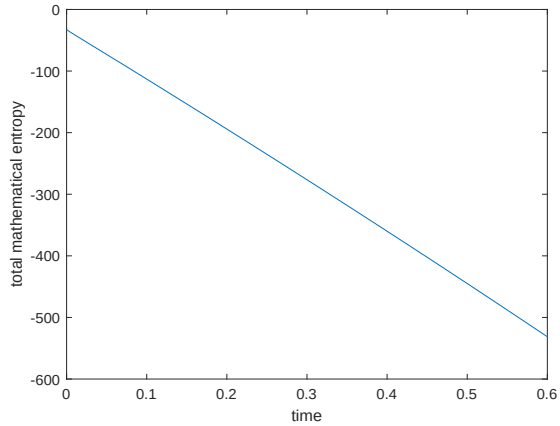

(e) Total mathematical entropy against time

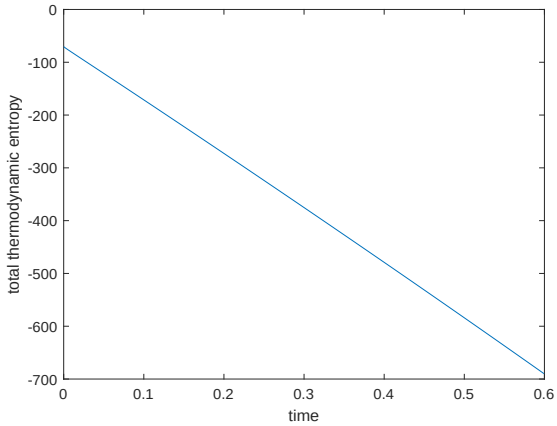

(f) Total thermodynamic entropy against time

Figure 6.6: Example 9: Density and pressure contours at $t = 0.6$ with $\Delta x = \Delta y = 1/32$ and the evaluation of the total entropies for the denotation diffraction problem.

Example 10. Finally, we focus on the detonation problem with multiple obstacles. The computational domain is $[0, 10]\times[0, 8.3]$ and two rectagular obstacles are located in $[1.3, 3.3]\times[0, 2.6]$ and $[5.1, 8.3]\times[0, 4.3]$ respectively. The initial condition is

$$(\rho, u, v, p, Y) = \begin{cases} (7, 0, 0, 200, 0), & x^2 + y^2 \leqslant 0.36, \\ (1, 0, 0, 55, 1), & x^2 + y^2 > 0.36 \end{cases} \tag{6.13}$$

and all the boundaries are solid walls.

To capture small structures near the corners we employ non-uniformly rectangular mesh, which is plotted in Fig. 6.7. CFL number is taken as 0.65. Numerical results at the terminal time $t = 1.4$ are given in Fig. 6.8, from which we can see that the complex detonation structures are resolved clearly without oscillations and both entropies decrease with time.

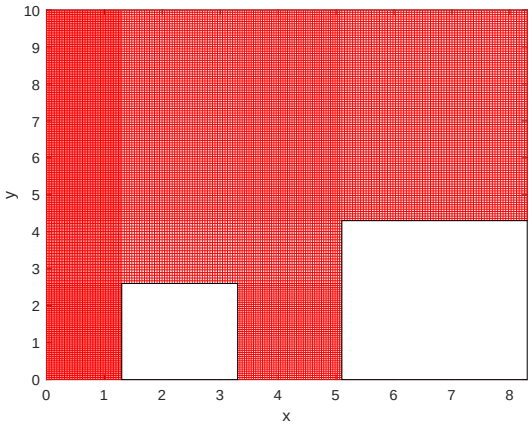

Figure 6.7: Example 10: The non-uniformly rectangular mesh for the detonation problem with multiple obstacles.

7. Concluding remarks

In this work, we construct a high order positivity preserving and oscillation-free entropy stable DG scheme for the reactive Euler equations. We first follow the framework of [19] to obtain an entropy stable DG scheme, where the flux proposed in [42] as the entropy conservative flux and the HLL flux [44] as the entropy stable flux. We prove that the flux

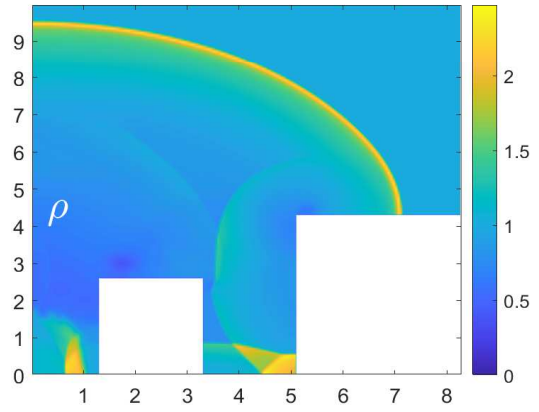

(a) Colored contour of density

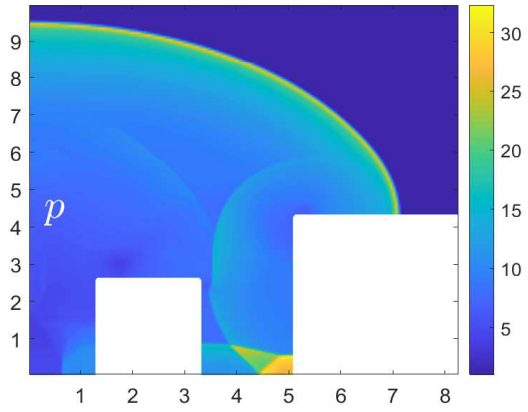

(b) Colored contour of pressure

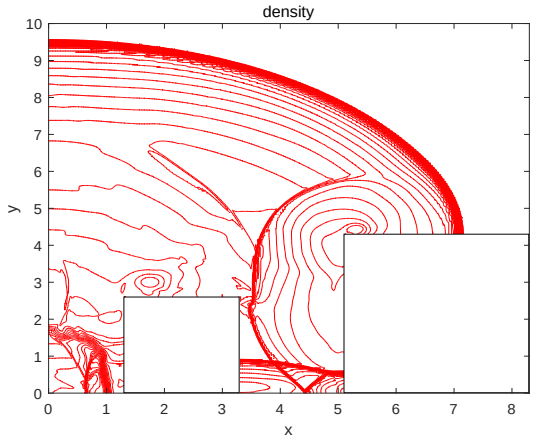

(c) 32 contour lines of density

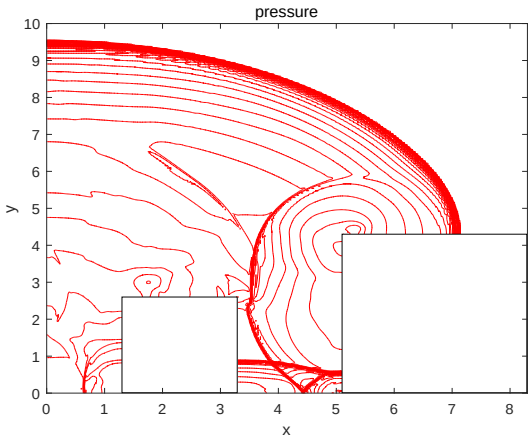

(d) 32 contour lines of pressure

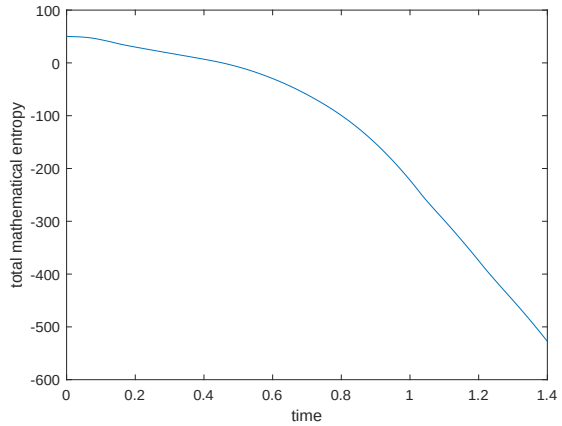

(e) Total mathematical entropy against time

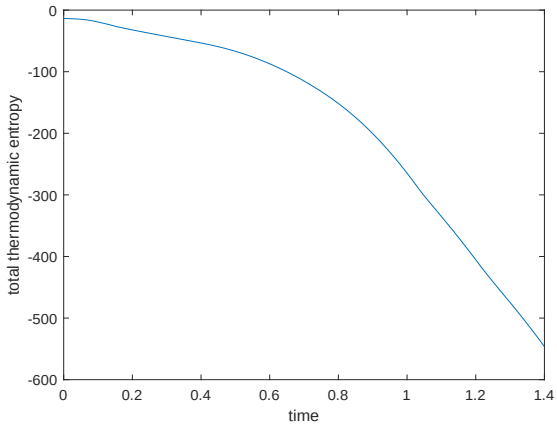

(f) Total thermodynamic entropy against time

Figure 6.8: Example 10: Density and pressure contours at $t = 1.4$ with non-uniformly rectangular mesh and the evaluation of the total entropies for the detonation problem with multiple obstacles.

in [42] is entropy conservative for both the thermodynamic and mathematical entropies and the HLL flux is entropy stable for both entropies under suitable estimations for the wave speeds. In this way, the DG scheme we obtain is entropy stable for both the thermodynamic and mathematical entropies. Additionally, damping terms are added as in [25] to restrain oscillations and the positivity preserving limiters in [9] are imposed to guarantee the positivity of the density, pressure and mass fraction. These ingredients are compatible with each other so that our scheme simultaneously enjoys the properties of entropy stable, oscillation-free and positivity preserving. We test the scheme via various 1D and 2D examples. The numerical results not only validate the designed high convergence orders of the scheme and but also demonstrate its good performances for discontinuous problems. Some extreme problems are also employed to show the necessity of positivity preserving limiters.

We would like to remark that since the entropy condition for the thermodynamic entropy corresponds to the second law of thermodynamics and that for the mathematical entropy is crucial for the wellposedness of solutions, our scheme is meaningful in both physics and mathematics. From this point of view, our scheme should be reliable in predicting complex detonation problems. We hope to extend the scheme to 3D and apply it to real applications in the future.

Appendix A. Proof of (3.32) and (3.33)

Proof. Recall that the variables $\mathbf{u}_{Euler}$ and the flux $\mathbf{f}_{Euler}(\mathbf{u}_{Euler})$ of the Euler equations are

$$\mathbf{u}_{Euler} = \begin{pmatrix} \rho \\ \rho u \\ \rho \tilde{E} \end{pmatrix} \tag{A.1}$$

and

$$\mathbf{f}_{Euler}(\mathbf{u}_{Euler}) = \begin{pmatrix} \rho u \\ \rho u^2 + p \\ (\rho \tilde{E} + p)u \end{pmatrix}. \tag{A.2}$$

The corresponding total energy $\rho\tilde{E}$ is determined by

$$\rho\tilde{E} = \frac{p}{\gamma - 1} + \frac{\rho u^2}{2} \tag{A.3}$$

and thus

$$\rho E = \rho\tilde{E} + q\rho Y. \tag{A.4}$$

With (A.1), (A.2) and (A.4), the variable $\mathbf{u}$ and the flux $\mathbf{f}(\mathbf{u})$ of the reactive Euler equations can be written as

$$\begin{aligned}
\mathbf{u} &= \begin{pmatrix} \mathbf{u}^1_{Euler} \\ \mathbf{u}^2_{Euler} \\ \mathbf{u}^3_{Euler} \\ 0 \end{pmatrix} + \begin{pmatrix} 0 \\ 0 \\ q\rho Y \\ \rho Y \end{pmatrix} := \mathbf{u}_1(\mathbf{u}) + \mathbf{u}_2(\mathbf{u}), \\
\mathbf{f}(\mathbf{u}) &= \begin{pmatrix} \mathbf{f}^1_{Euler} \\ \mathbf{f}^2_{Euler} \\ \mathbf{f}^3_{Euler} \\ 0 \end{pmatrix} + \begin{pmatrix} 0 \\ 0 \\ q\rho u Y \\ \rho u Y \end{pmatrix} := \mathbf{f}_1(\mathbf{u}) + \mathbf{f}_2(\mathbf{u}),
\end{aligned} \tag{A.5}$$

where $\mathbf{u}^i_{Euler}$ and $\mathbf{f}^i_{Euler}$ are the i-th component of $\mathbf{u}_{Euler}$ and $\mathbf{f}_{Euler}$, respectively.

On the other hand, we denote $\lambda^+_R = \max(\lambda_R, 0)$ and $\lambda^-_L = \min(\lambda_L, 0)$ and rewrite the HLL flux (3.29) as

$$\begin{aligned}
\hat{\mathbf{f}}(\mathbf{u}_L, \mathbf{u}_R) =& \frac{\lambda^+_R \mathbf{f}(\mathbf{u}_L) - \lambda^-_L \mathbf{f}(\mathbf{u}_R) + \lambda^-_L \lambda^+_R (\mathbf{u}_R - \mathbf{u}_L)}{\lambda^+_R - \lambda^-_L} \\
=& \frac{\lambda^+_R \mathbf{f}_1(\mathbf{u}_L) - \lambda^-_L \mathbf{f}_1(\mathbf{u}_R) + \lambda^-_L \lambda^+_R (\mathbf{u}_1(\mathbf{u}_R) - \mathbf{u}_1(\mathbf{u}_L))}{\lambda^+_R - \lambda^-_L} \\
&+ \frac{\lambda^+_R \mathbf{f}_2(\mathbf{u}_L) - \lambda^-_L \mathbf{f}_2(\mathbf{u}_R) + \lambda^-_L \lambda^+_R (\mathbf{u}_2(\mathbf{u}_R) - \mathbf{u}_2(\mathbf{u}_L))}{\lambda^+_R - \lambda^-_L}.
\end{aligned}$$

Then it follows that

$$\begin{aligned}
&(\hat{\mathbf{v}}_R - \hat{\mathbf{v}}_L)^T \hat{\mathbf{f}}(\mathbf{u}_L, \mathbf{u}_R) \\
=& (\hat{\mathbf{v}}_R - \hat{\mathbf{v}}_L)^T \frac{\lambda^+_R \mathbf{f}_1(\mathbf{u}_L) - \lambda^-_L \mathbf{f}_1(\mathbf{u}_R) + \lambda^-_L \lambda^+_R (\mathbf{u}_1(\mathbf{u}_R) - \mathbf{u}_1(\mathbf{u}_L))}{\lambda^+_R - \lambda^-_L} \\
&+ (\hat{\mathbf{v}}_R - \hat{\mathbf{v}}_L)^T \frac{\lambda^+_R \mathbf{f}_2(\mathbf{u}_L) - \lambda^-_L \mathbf{f}_2(\mathbf{u}_R) + \lambda^-_L \lambda^+_R (\mathbf{u}_2(\mathbf{u}_R) - \mathbf{u}_2(\mathbf{u}_L))}{\lambda^+_R - \lambda^-_L}.
\end{aligned} \tag{A.6}$$

Noticing that the last entry of $\mathbf{f}_1(\mathbf{u})$ is zero, we compute the first term in (A.6) as

$$\begin{aligned}
&(\hat{\mathbf{v}}_R - \hat{\mathbf{v}}_L)^T \frac{\lambda_R^+ \mathbf{f}_1(\mathbf{u}_L) - \lambda_L^- \mathbf{f}_1(\mathbf{u}_R) + \lambda_L^- \lambda_R^+ (\mathbf{u}_1(\mathbf{u}_R) - \mathbf{u}_1(\mathbf{u}_L))}{\lambda_R^+ - \lambda_L^-} \\
&= (\hat{\mathbf{v}}_{Euler,R} - \hat{\mathbf{v}}_{Euler,L})^T \frac{\lambda_R^+ \mathbf{f}_{Euler}(\mathbf{u}_{Euler,L}) - \lambda_L^- \mathbf{f}_{Euler}(\mathbf{u}_{Euler,R}) + \lambda_L^- \lambda_R^+ (\mathbf{u}_{Euler,R} - \mathbf{u}_{Euler,L})}{\lambda_R^+ - \lambda_L^-} \\
&= (\hat{\mathbf{v}}_{Euler,R} - \hat{\mathbf{v}}_{Euler,L})^T \widehat{\mathbf{f}}_{Euler}(\mathbf{u}_{Euler,L}, \mathbf{u}_{Euler,R}).
\end{aligned} \tag{A.7}$$

Moreover, observe that $\hat{\mathbf{v}}$ in (3.22) has the structure

$$(\star, \star, a, -qa)^T \tag{A.8}$$

and that $\mathbf{u}_2(\mathbf{u})$ and $\mathbf{f}_2(\mathbf{u})$ defined in (A.5) both have the structure

$$(0, 0, qb, b)^T. \tag{A.9}$$

Then $\hat{\mathbf{v}}_{Euler,R} - \hat{\mathbf{v}}_{Euler,L}$, $\hat{\mathbf{v}}_R - \hat{\mathbf{v}}_L$ and the second term in (A.6) also possess the structure (A.8) and (A.9), respectively. Thus we have

$$(\hat{\mathbf{v}}_R - \hat{\mathbf{v}}_L)^T \frac{\lambda_R^+ \mathbf{f}_2(\mathbf{u}_L) - \lambda_L^- \mathbf{f}_2(\mathbf{u}_R) + \lambda_L^- \lambda_R^+ (\mathbf{u}_2(\mathbf{u}_R) - \mathbf{u}_2(\mathbf{u}_L))}{\lambda_R^+ - \lambda_L^-} = 0. \tag{A.10}$$

Combining (A.7) and (A.10) yields

$$\begin{aligned}
\Delta_{T,HLL} &= (\hat{\mathbf{v}}_R - \hat{\mathbf{v}}_L)^T \widehat{\mathbf{f}}(\mathbf{u}_L, \mathbf{u}_R) - (\rho u)_R + (\rho u)_L \\
&= (\hat{\mathbf{v}}_{Euler,R} - \hat{\mathbf{v}}_{Euler,L})^T \widehat{\mathbf{f}}_{Euler}(\mathbf{u}_{Euler,L}, \mathbf{u}_{Euler,R}) - (\rho u)_R + (\rho u)_L \\
&= \Delta_{Euler,HLL},
\end{aligned} \tag{A.11}$$

and thereby (3.32) is proved.

To prove (3.33), we decompose the entropy variable $\mathbf{v}$ in (2.6) as

$$\mathbf{v} = \hat{\mathbf{v}} + \begin{pmatrix} -Y^2 \\ 0 \\ 0 \\ 2Y \end{pmatrix} := \hat{\mathbf{v}} + \mathbf{v}_1.$$

With this and (A.11), it is direct to verify that

$$\begin{aligned}\Delta_{M,HLL} &:= (\mathbf{v}_R - \mathbf{v}_L)^T \widehat{\mathbf{f}}(\mathbf{u}_L, \mathbf{u}_R) - (\rho u)_R + (\rho u)_L \\ &= (\hat{\mathbf{v}}_R - \hat{\mathbf{v}}_L)^T \widehat{\mathbf{f}}(\mathbf{u}_L, \mathbf{u}_R) - (\rho u)_R + (\rho u)_L + (\mathbf{v}_{1,R} - \mathbf{v}_{1,L})^T \widehat{\mathbf{f}}(\mathbf{u}_L, \mathbf{u}_R) \\ &= \Delta_{T,HLL} + (\mathbf{v}_{1,R} - \mathbf{v}_{1,L})^T \widehat{\mathbf{f}}(\mathbf{u}_L, \mathbf{u}_R).\end{aligned}$$

Next we to compute the second term in the above equation as

$$\begin{aligned}&(\mathbf{v}_{1,R} - \mathbf{v}_{1,L})^T \widehat{\mathbf{f}}(\mathbf{u}_L, \mathbf{u}_R) \\ =&(-Y_R^2 + Y_L^2, 0, 0, 2Y_R - 2Y_L)^T \frac{\lambda_R^+ \mathbf{f}(\mathbf{u}_L) - \lambda_L^- \mathbf{f}(\mathbf{u}_R) + \lambda_L^- \lambda_R^+ (\mathbf{u}_R - \mathbf{u}_L)}{\lambda_R^+ - \lambda_L^-} \\ =&\frac{Y_R - Y_L}{\lambda_R^+ - \lambda_L^-} \big\{ -(Y_R + Y_L)[\lambda_R^+ \rho_L (u_L - \lambda_L^-) - \lambda_L^- \rho_R (u_R - \lambda_R^+)] \\ &\qquad +2[\lambda_R^+ \rho_L Y_L (u_L - \lambda_L^-) - \lambda_L^- \rho_R Y_R (u_R - \lambda_R^+)] \big\} \\ =&\frac{(Y_R - Y_L)^2}{\lambda_R^+ - \lambda_L^-} \left[\lambda_R^+ \rho_L (\lambda_L^- - u_L) + \lambda_L^- \rho_R (\lambda_R^+ - u_R) \right].\end{aligned}$$

The above two equations yield (3.33). □

Appendix B. Proof of Lemma 4.1 and 4.2 and Theorem 4.1

To begin with, we introduce the following lemma, the proof of which is straightforward.

Lemma Appendix B.1. *For the reactive Euler equations* (2.1)*, we have the following lemma.*

(1) *If* $\mathbf{u} \in G$*, then* $k\mathbf{u} \in G$ *for any* $k > 0$*.*

(2) *If* $\mathbf{u}_1$ *and* $\mathbf{u}_2 \in G$*, then* $a\mathbf{u}_1 + b\mathbf{u}_2 \in G$ *for any* $a, b > 0$*.*

(3) *If* $\mathbf{u} \in G$*, then* $\alpha\mathbf{u} - \mathbf{f}(\mathbf{u}) \in G$ *for any* $\alpha \geq u + c$ *and* $-\beta\mathbf{u} + \mathbf{f}(\mathbf{u}) \in G$ *for any* $\beta \leq u - c$*.*

Proof of Lemma 4.1. Set S_{R_1} and S_{L_1} as the approximations of the rightmost and leftmost wave speeds in the HLL flux (3.29) at the interface $x_{i+1/2}$, respectively. Denote $S_{R_1}^+ = \max(0, S_{R_1})$ and $S_{L_1}^- = \min(0, S_{L_1})$. Similarly, we define $S_{R_2}^+$ and $S_{L_2}^-$ at the interface $x_{i-1/2}$.

It is straightforward to compute from the first order finite volume scheme (4.1) that

$$\begin{aligned}
\mathbf{u}_i^{n+1} &= \mathbf{u}_i^n - \lambda\hat{\mathbf{f}}(\mathbf{u}_i^n, \mathbf{u}_{i+1}^n) + \lambda\hat{\mathbf{f}}(\mathbf{u}_{i-1}^n, \mathbf{u}_i^n) \\
&= \mathbf{u}_i^n - \lambda\frac{S_{R_1}^+\mathbf{f}(\mathbf{u}_i^n) - S_{L_1}^-\mathbf{f}(\mathbf{u}_{i+1}^n) + S_{R_1}^+S_{L_1}^-(\mathbf{u}_{i+1}^n - \mathbf{u}_i^n)}{S_{R_1}^+ - S_{L_1}^-} \\
&+ \lambda\frac{S_{R_2}^+\mathbf{f}(\mathbf{u}_{i-1}^n) - S_{L_2}^-\mathbf{f}(\mathbf{u}_i^n) + S_{R_2}^+S_{L_2}^-(\mathbf{u}_i^n - \mathbf{u}_{i-1}^n)}{S_{R_2}^+ - S_{L_2}^-} \\
&= \left[\left(1 + \frac{\lambda S_{L_1}^- S_{R_1}^+}{S_{R_1}^+ - S_{L_1}^-} + \frac{\lambda S_{R_2}^+ S_{L_2}^-}{S_{R_2}^+ - S_{L_2}^-}\right)\mathbf{u}_i^n - \left(\frac{\lambda S_{R_1}^+}{S_{R_1}^+ - S_{L_1}^-} + \frac{\lambda S_{L_2}^-}{S_{R_2}^+ - S_{L_2}^-}\right)\mathbf{f}(\mathbf{u}_i^n)\right] \\
&+ \left(\frac{-\lambda S_{L_1}^-}{S_{R_1}^+ - S_{L_1}^-}\right)\left(S_{R_1}^+\mathbf{u}_{i+1}^n - \mathbf{f}(\mathbf{u}_{i+1}^n)\right) + \left(\frac{\lambda S_{R_2}^+}{S_{R_2}^+ - S_{L_2}^-}\right)\left(-S_{L_2}^+\mathbf{u}_{i-1}^n + \mathbf{f}(\mathbf{u}_{i-1}^n)\right) \\
&:= A_1 + A_2 + A_3.
\end{aligned} \tag{B.1}$$

According to Lemma Appendix B.1, it suffices to prove $A_1, A_2, A_3 \in G$, where $A_2, A_3 \in G$ is obvious under the condition (4.2). In the following, we show $A_1 \in G$.

Denote $a = \frac{S_{R_1}^+}{S_{R_1}^+ - S_{L_1}^-} \in [0,1]$ and $b = \frac{S_{L_2}^-}{S_{R_2}^+ - S_{L_2}^-} \in [-1,0]$. Then

$$A_1 = (1 + \lambda S_{L_1}^- a + \lambda S_{R_2}^+ b)\mathbf{u}_i^n - \lambda(a+b)\mathbf{f}(\mathbf{u}_i^n).$$

Here we discuss three cases of $a + b$.

(1) $a + b = 0$.

In this case, $A_1 = [1 + \lambda(S_{R_2}^+ - S_{L_1}^-)b]\mathbf{u}_i^n$ and we turn to show the coefficient $1 + \lambda(S_{R_2}^+ - S_{L_1}^-)b > 0$. Note that $b \in [-1, 0]$ and thus we have

$$1 + \lambda(S_{R_2}^+ - S_{L_1}^-)b \geq 1 + 2\lambda b a_0 \geq 1 - 2\lambda a_0 \geq 0,$$

where the last inequality is due to the CFL condition $\lambda a_0 \leq 1/2$. The equalities in the above equation hold only if

$$S_{R_2}^+ - S_{L_1}^- = 2a_0, \quad b = -1.$$

That implies that $a_0 = 0$, which is impossible. Thus $1 + \lambda(S_{R_2}^+ - S_{L_1}^-)b > 0$ and $A_1 \in G$.

(2) $a+b>0$.

In this case, we have

$$A_1=\lambda(a+b)[\frac{1+\lambda S^+_{L_1}a+\lambda S^+_{R_2}b}{\lambda(a+b)}\mathbf{u}_i^n+\mathbf{f}(\mathbf{u}_i^n)]$$

and turn to show that

$$\frac{1+\lambda S^+_{L_1}a+\lambda S^+_{R_2}b}{\lambda(a+b)}\geq u_i+c_i. \tag{B.2}$$

We directly compute

$$\begin{aligned}
&1+\lambda a(S^-_{L_1}-u_i-c_i)+\lambda b(S^+_{R_2}-u_i-c_i)\\
=&1+\lambda a(S^-_{L_1}-u_i-c_i)+\lambda(a+b)(S^+_{R_2}-u_i-c_i)-\lambda a(S^+_{R_2}-u_i-c_i)\\
\geq&1+\lambda a(S^-_{L_1}-u_i-c_i)-\lambda a(S^+_{R_2}-u_i-c_i)\\
=&1+\lambda a(S^-_{L_1}-S^+_{R_2})\\
\geq&1-2a_0\lambda\geq 0,
\end{aligned}$$

where the first inequality is due to the condition (4.2) and the last inequality is because of the CFL condition $\lambda a_0\leq 1/2$. This leads to (B.2).

(3) $a+b<0$.

This case is similar to the case (2) and we skip the proof.

Combining the above three cases, we obtain $A_1\in G$ and thus $\mathbf{u}_i^{n+1}\in G$. □

Proof of Lemma 4.2. Based on Lemma 4.1, the proof of Lemma 4.2 is the same as that of Theorem 2.1 in [22]. □

Proof of Theorem 4.1. We compute from the scheme (4.4) that

$$\begin{aligned}
\bar{\mathbf{u}}^{i,n+1} &= \bar{\mathbf{u}}^{i,n} - \lambda\left[\hat{\mathbf{f}}(\mathbf{u}^-_{i+1/2},\mathbf{u}^+_{i+1/2}) - \hat{\mathbf{f}}(\mathbf{u}^-_{i-1/2},\mathbf{u}^+_{i-1/2})\right] + \Delta t\bar{\mathbf{s}}^{i,n} \\
&= \bar{\mathbf{u}}^{i,n} - \lambda\left[\hat{\mathbf{f}}(\mathbf{u}^-_{i+1/2},\mathbf{u}^+_{i+1/2}) - \hat{\mathbf{f}}(\mathbf{u}^-_{i-1/2},\mathbf{u}^+_{i-1/2})\right] + \frac{\Delta t}{2}\sum_{j=0}^{k}\omega_j\mathbf{s}(\mathbf{u}_j^{i,n}) \\
&= \frac{1}{2}\left\{\bar{\mathbf{u}}^{i,n} - 2\lambda\left[\hat{\mathbf{f}}(\mathbf{u}^-_{i+1/2},\mathbf{u}^+_{i+1/2}) - \hat{\mathbf{f}}(\mathbf{u}^-_{i-1/2},\mathbf{u}^+_{i-1/2})\right]\right\} + \frac{1}{2}\left[\bar{\mathbf{u}}^{i,n} + \Delta t\sum_{j=0}^{k}\omega_j\mathbf{s}(\mathbf{u}_j^{i,n})\right] \\
&= \frac{1}{2}\left\{\bar{\mathbf{u}}^{i,n} - 2\lambda\left[\hat{\mathbf{f}}(\mathbf{u}^-_{i+1/2},\mathbf{u}^+_{i+1/2}) - \hat{\mathbf{f}}(\mathbf{u}^-_{i-1/2},\mathbf{u}^+_{i-1/2})\right]\right\} + \frac{1}{4}\sum_{j=0}^{k}\omega_j\left[\mathbf{u}_j^{i,n} + 2\Delta t\mathbf{s}(\mathbf{u}_j^{i,n})\right].
\end{aligned} \tag{B.3}$$

According to the Lemma 3.1 and Theorem 4.2, if $\lambda a_0 \le \frac{1}{8}\omega_0$ and $\mathbf{u}_j^{i,n} + 2\Delta t\mathbf{s}(\mathbf{u}_j^{i,n}) \in G$, then $\bar{\mathbf{u}}^{i,n+1} \in G$. Here $\mathbf{u}_j^{i,n} + 2\Delta t\mathbf{s}(\mathbf{u}_j^{i,n}) \in G$ is equivalent to $\max_{i,j}\{\Delta t\tilde{K}e^{-\tilde{T}/T_j^{i,n}}\} \le \frac{1}{2}$. This completes the proof. □

Acknowledgements

We thank the reviewers for helpful comments and suggestions, which enable us to significantly improve the quality of the paper. This work was supported by the National Natural Science Foundation of China (Grant Nos. 12371388 and 12071246).

References

[1] Barna Bihari and Donald Schwendeman. Multiresolution schemes for the reactive Euler equations. Journal of Computational Physics, 154:197–230, 1999.

[2] Min Xiao, Guoxi Ni, Cheng Wang, and Tonghui Yang. Front capturing by level set method for the reactive Euler equations. International Journal for Numerical Methods in Fluids, 93(8):2723–2743, 2021.

[3] Zhen-Hua Jiang, Xi Deng, Chao Yan, Feng Xiao, and Jian Yu. Positivity-preserving

hybrid DG/FV method with subcell resolution for compressible Euler equations with stiff source terms. arXiv preprint arXiv:2007.05867, 2020.

[4] Magnus Svärd and Siddhartha Mishra. Implicit–explicit schemes for flow equations with stiff source terms. Journal of Computational and Applied Mathematics, 235(6):1564–1577, 2011.

[5] Luca Tosatto and Luigi Vigevano. Numerical solution of under-resolved detonations. Journal of Computational Physics, 227(4):2317–2343, 2008.

[6] Weizhu Bao and Shi Jin. The random projection method for hyperbolic conservation laws with stiff reaction terms. Journal of Computational Physics, 163(1):216–248, 2000.

[7] Christiane Helzel, Randall J. Leveque, and Gerald Warnecke. A modified fractional step method for the accurate approximation of detonation waves. SIAM Journal on Scientific Computing, 22(4):1489–1510, 2000.

[8] Matania Ben-Artzi. The generalized Riemann problem for reactive flows. Journal of Computational physics, 81(1):70–101, 1989.

[9] Cheng Wang, Xiangxiong Zhang, Chi-Wang Shu, and Jianguo Ning. Robust high order discontinuous Galerkin schemes for two-dimensional gaseous detonations. Journal of Computational Physics, 231(2):653–665, 2012.

[10] Yimin Lin, Jesse Chan, and Ignacio Tomas. A positivity preserving strategy for entropy stable discontinuous Galerkin discretizations of the compressible Euler and Navier-Stokes equations. Journal of Computational Physics, 475:111850, 2023.

[11] Stanley Osher and Eitan Tadmor. On the convergence of difference approximations to scalar conservation laws. Mathematics of Computation, 50(181):19–51, 1988.

[12] Eitan Tadmor. The numerical viscosity of entropy stable schemes for systems of conservation laws. I. Mathematics of Computation, 49(179):91–103, 1987.

[13] Eitan Tadmor. Entropy stability theory for difference approximations of nonlinear conservation laws and related time-dependent problems. Acta Numerica, 12:451–512, 2003.

[14] Ulrik S Fjordholm, Siddhartha Mishra, and Eitan Tadmor. Arbitrarily high-order accurate entropy stable essentially nonoscillatory schemes for systems of conservation laws. SIAM Journal on Numerical Analysis, 50(2):544–573, 2012.

[15] Xiangxiong Zhang and Chi-Wang Shu. Positivity-preserving high order finite difference WENO schemes for compressible Euler equations. Journal of Computational Physics, 231(5):2245–2258, 2012.

[16] Bernardo Cockburn, George E Karniadakis, and Chi-Wang Shu. The development of discontinuous Galerkin methods. Lecture Notes in Computational Science and Engineering, 11:3–50, 2000.

[17] Guangshan Jiang and Chi-Wang Shu. On a cell entropy inequality for discontinuous Galerkin methods. Mathematics of Computation, 62(206):531–538, 1994.

[18] Songming Hou and Xu-Dong Liu. Solutions of multi-dimensional hyperbolic systems of conservation laws by square entropy condition satisfying discontinuous Galerkin method. Journal of Scientific Computing, 31:127–151, 2007.

[19] Tianheng Chen and Chi-Wang Shu. Entropy stable high order discontinuous Galerkin methods with suitable quadrature rules for hyperbolic conservation laws. Journal of Computational Physics, 345:427–461, 2017.

[20] David C Del Rey Fernández, Jason E Hicken, and David W Zingg. Simultaneous approximation terms for multi-dimensional summation-by-parts operators. Journal of Scientific Computing, 75:83–110, 2018.

[21] Jason E Hicken, David C Del Rey Fernández, and David W Zingg. Multidimensional summation-by-parts operators: general theory and application to simplex elements. SIAM Journal on Scientific Computing, 38(4):A1935–A1958, 2016.

[22] Xiangxiong Zhang and Chi-Wang Shu. On positivity-preserving high order discontinuous Galerkin schemes for compressible Euler equations on rectangular meshes. Journal of Computational Physics, 229(23):8918–8934, 2010.

[23] Xiangxiong Zhang, Yinhua Xia, and Chi-Wang Shu. Maximum-principle-satisfying and positivity-preserving high order discontinuous Galerkin schemes for conservation laws on triangular meshes. Journal of Scientific Computing, 50(1):29–62, 2012.

[24] Xiangxiong Zhang and Chi-Wang Shu. Positivity-preserving high order discontinuous Galerkin schemes for compressible Euler equations with source terms. Journal of Computational Physics, 230(4):1238–1248, 2011.

[25] Yong Liu, Jianfang Lu, and Chi-Wang Shu. An entropy stable oscillation-free discontinuous Galerkin method for hyperbolic conservation laws. https://bpb-us-w2.wpmucdn.com/sites.brown.edu/dist/0/348/files/2022/09/An-entropy-st preprint.

[26] Jianfang Lu, Yong Liu, and Chi-Wang Shu. An oscillation-free discontinuous Galerkin method for scalar hyperbolic conservation laws. SIAM Journal on Numerical Analysis, 59(3):1299–1324, 2021.

[27] Yong Liu, Jianfang Lu, and Chi-Wang Shu. An essentially oscillation-free discontinuous Galerkin method for hyperbolic systems. SIAM Journal on Scientific Computing, 44(1):A230–A259, 2022.

[28] Yong Liu, Jianfang Lu, Qi Tao, and Yinhua Xia. An oscillation-free discontinuous Galerkin method for shallow water equations. Journal of Scientific Computing, 92(109):1–24, 2022.

[29] Qi Tao, Yong Liu, Yan Jiang, and Jianfang Lu. An oscillation free local discontinuous Galerkin method for nonlinear degenerate parabolic equations. Numerical Method for Partial Differential Equations, 39(4):3145–3169, 2023.

[30] Jie Du, Yong Liu, and Yang Yang. An oscillation-free bound-preserving discontinuous Galerkin method for multi-component chemically reacting flows. Journal of Scientific Computing, 95(3):90, 2023.

[31] Jesse Chan, David C Del Rey Fernández, and Mark H Carpenter. Efficient entropy stable Gauss collocation methods. SIAM Journal on Scientific Computing, 41(5):A2938–A2966, 2019.

[32] Jesse Chan. On discretely entropy conservative and entropy stable discontinuous Galerkin methods. Journal of Computational Physics, 362:346–374, 2018.

[33] Jared Crean, Jason E Hicken, David C Del Rey Fernández, David W Zingg, and Mark H Carpenter. High-order, entropy-stable discretizations of the Euler equations for complex

geometries. In 23rd AIAA computational fluid dynamics conference. American Institute of Aeronautics and Astronautics, 2017.

[34] Jared Crean, Jason E Hicken, David C Del Rey Fernández, David W Zingg, and Mark H Carpenter. Entropy-stable summation-by-parts discretization of the Euler equations on general curved elements. Journal of Computational Physics, 356:410–438, 2018.

[35] Lucas Friedrich, Gero Schnücke, Andrew R Winters, David C Del Rey Fernández, Gregor J Gassner, and Mark H Carpenter. Entropy stable space–time discontinuous Galerkin schemes with summation-by-parts property for hyperbolic conservation laws. Journal of Scientific Computing, 80:175–222, 2019.

[36] Lucas Friedrich, Andrew R Winters, David C Del Rey Fernández, Gregor J Gassner, Matteo Parsani, and Mark H Carpenter. An entropy stable h/p non-conforming discontinuous Galerkin method with the summation-by-parts property. Journal of Scientific Computing, 77:689–725, 2018.

[37] Marvin Bohm, Andrew R Winters, Gregor J Gassner, Dominik Derigs, Florian Hindenlang, and Joachim Saur. An entropy stable nodal discontinuous Galerkin method for the resistive MHD equations. Part I: Theory and numerical verification. Journal of Computational Physics, 422:108076, 2020.

[38] Jesse Chan and Lucas C Wilcox. On discretely entropy stable weight-adjusted discontinuous Galerkin methods: curvilinear meshes. Journal of Computational Physics, 378:366–393, 2019.

[39] Gregor J Gassner, Andrew R Winters, Florian J Hindenlang, and David A Kopriva. The

BR1 scheme is stable for the compressible Navier–Stokes equations. Journal of Scientific Computing, 77:154–200, 2018.

[40] Jan Glaubitz, Jan Nordström, and Philipp Öffner. Summation-by-parts operators for general function spaces. SIAM Journal on Numerical Analysis, 61(2):733–754, 2023.

[41] Jan Glaubitz, Simon-Christian Klein, Jan Nordström, and Philipp Öffner. Multi-dimensional summation-by-parts operators for general function spaces: Theory and construction. arXiv preprint arXiv:2301.12996, 2023.

[42] Weifeng Zhao. Strictly convex entropy and entropy stable schemes for reactive Euler equations. Mathematics of Computation, 91:735–760, 2021.

[43] Wen-An Yong. Entropy and global existence for hyperbolic balance laws. Archive for Rational Mechanics and Analysis, 172:247–266, 2004.

[44] Amiram Harten, Peter D Lax, and Bram van Leer. On upstream differencing and Godunov-type schemes for hyperbolic conservation laws. SIAM Review, 25(1):35–61, 1983.

[45] Praveen Chandrashekar. Kinetic energy preserving and entropy stable finite volume schemes for compressible Euler and Navier-Stokes equations. Communications in Computational Physics, 14(5):1252–1286, 2013.

[46] Farzad Ismail and Philip L Roe. Affordable, entropy-consistent Euler flux functions II: Entropy production at shocks. Journal of Computational Physics, 228(15):5410–5436, 2009.

[47] Chi-Wang Shu and Stanley Osher. Efficient implementation of essentially non-oscillatory shock-capturing schemes. Journal of Computational Physics, 77(2):439–471, 1988.

[48] Raymond J. Spiteri and Steven J. Ruuth. A new class of optimal high-order Strong-Stability-Preserving time discretization methods. SIAM Journal on Numerical Analysis, 40(2):469–491, 2002.

[49] Juntao Huang and Chi-Wang Shu. Bound-preserving modified exponential Runge–Kutta discontinuous Galerkin methods for scalar hyperbolic equations with stiff source terms. Journal of Computational Physics, 361:111–135, 2018.

[50] Jie Du, Cheng Wang, Chengeng Qian, and Yang Yang. High-order bound-preserving discontinuous Galerkin methods for stiff multispecies detonation. SIAM Journal on Scientific Computing, 41(2):B250–B273, 2019.

[51] Jie Du and Yang Yang. Third-order conservative sign-preserving and steady-state preserving time integrations and applications in stiff multispecies and multireaction detonations. Journal of Computational physics, 395:489–510, 2019.

[52] Chi-Wang Shu and Stanley Osher. Efficient implementation of essentially non-oscillatory shock-capturing schemes, II. Journal of Computational Physics, 83(1):32–78, 1989.

[53] Manting Peng, Zheng Sun, and Kailiang Wu. OEDG: Oscillation-eliminating discontinuous galerkin method for hyperbolic conservation laws. arXiv preprint arXiv:2310.04807, 2023.

[54] Timur Linde and Philip Roe. Robust Euler codes. In 13th Computational Fluid Dynamics Conference, 1997.

[55] Xianyang Zeng, Min Xiao, and Guoxi Ni. An efficient numerical method for reactive flow with general equation of states. International Journal for Numerical Methods in Fluids, 82(10):631–645, 2016.

[56] Bernardo Cockburn, San-Yih Lin, and Chi-Wang Shu. TVB Runge-Kutta local projection discontinuous Galerkin finite element method for conservation laws III: one-dimensional systems. Journal of Computational Physics, 84(1):90–113, 1989.